Oline Eiksund

# Performance Prediction and Design Modification of a Ship in Waves Using Computational Fluid Dynamics

Master's thesis in Ship Design
Supervisor: Henry Peter Piehl

June 2020

**Master's thesis**

**NTNU**
Norwegian University of Science and Technology
Faculty of Engineering
Department of Ocean Operations and Civil Engineering

**NTNU**
Norwegian University of
Science and Technology

Oline Eiksund

# Performance Prediction and Design Modification of a Ship in Waves Using Computational Fluid Dynamics

Master's thesis in Ship Design
Supervisor: Henry Peter Piehl
June 2020

Norwegian University of Science and Technology
Faculty of Engineering
Department of Ocean Operations and Civil Engineering

**NTNU**
Norwegian University of
Science and Technology

# Abstract

The ship design industry is constantly developing, and the focus around performance and efficiency keeps getting more important. How the ships behaves due to the interaction of external loads affects the comfort level experienced on board, and especially in heavy seas, it can be hard to maintain the comfort requirements. This master thesis focuses on the performance prediction for ship in waves, and hull design modification by using computational fluid dynamics.

Based on an original hull design, a modified design aiming to improve the sea performance was modeled. These two hull designs was tested for a set of different wave lengths and wave heights relevant for the trade route by using CFD simulations. The results was used to evaluate if the design could benefit from being adjusted, and if CFD analysis have the potential to capture the difference in the design stage.

The hull designs was modeled in Siemens NX, the CFD analysis was performed by using Star CCM+, and the final results was handled in Python and Matlab. The final results is presented as a comparison between the original hull design and the modified hull design with regard to calm water resistance and ship motions.

# Sammendrag

Skipsdesignsindustrien utvikler seg hele tiden, og fokuset rundt ytelse og effektivitet blir stadig viktigere. Hvordan skipet responderer til eksterne krefter påvirker komfortnivået ombord, og spesielt i tøff sjø kan det være vanskelig å opprettholde komfortnivået og lastintegriteten. Hovedfokuset i denne masteroppgaven er ytelsesprediksjon for skip i bølger, og modifikasjon av skrogdesign ved hjelp av CFD analyser.

Basert på et skrogdesign, ble et modifisert design laget for å forbedre sjøegenskapene til skipet. Begge disse skrogene ble testet for flere forskjellige bølgelengder og bølgehøyder som var relevante for en bestemt rute ved å bruke CFD analyser. Resultatene ble brukt til å vurdere om skrogdesignet kunne dra nytte av å bli modifisert, og om CFD analyser hadde potensial til å fange opp designforskjellen i en tidlig designfase.

Skrogene ble modelert i Siemens NX, CFD analysene ble gjennomført ved å bruke Star CCM+, og sluttresultatene ble håndtert i Python og i Matlab. Resultatene ble presentert som en sammenligning mellom originaldesignet og det modifiserte skrogdesignet med hensyn til skrogmotstand og skipsbevegelser.

# Acknowledgments

# Table of Contents

# TABLE OF CONTENTS

# List of Figures

# List of Tables

# Nomenclature

**Abbreviations**

$C_B$    Block Coefficient

$CAD$  Computer Aided Design

$CFD$  Computational Fluid Dynamics

$CFL$  Courant–Friedrichs–Lewy Condition

$DFBI$  Dynamic Fluid Body Interaction

$DOF$  Degrees of Freedom

$FVM$  Finite Volume Discretization Method

$GM$   Metacentric Height

$LOA$  Length Over All

$LPP$  Length Between Perpendicular

$NS$   Navier Stokes

$PDE$  Partial Differential Equations

$RANS$  Reynolds Average Navier Stokes

$Re$    Reynolds Number

$RoPax$  Roll on/Roll off-Passenger-Ship

$VOF$  Volume of Fluid

## Other Symbols

$\ddot{\eta}$        Acceleration

$\dot{\eta}$        Velocity

$\mu$        Dynamic Viscosity

$\nu$        Kinematic Viscosity

$\rho$        Density

$c$        Phase Velocity

$F$        Force

$g$        Gravitational Constant

$H_S$        Significant Wave Height

$k$        Wave Number

$T$        Wave Period

$y^{+}$        Dimensionless Wall Distance

$\eta$        Displacement

# Chapter 1

# Introduction

## 1.1   Background

Ship performance are becoming more important, especially in segments where operating margins are low, and the emission regulations keeps getting tighter. Computational Fluid Dynamics (CFD) in ship design can provide key information of forces acting on the ship hull, the ships motion and hydrodynamic performance, and allows for an easier understanding of small design changes, just in a short amount of time after the change is done.

A Roll-on/Roll-off-Passenger-Ship (RoPax) is a vessel carrying both vehicles and passengers. This market face several strict requirements, and the vessels are operating in well defined sea conditions, often harsh climatic conditions. As the vessels are carrying both passengers and vehicles, this leads to strict requirements considering safety and comfort, as well as keeping the time schedule.

The inverted bow design X-Bow® is a design developed by Ulstein Design and Solutions. The design is per now mostly used on offshore vessels, but the company are exploring the opportunity to improve the design further to optimize it for the RoPax segment as well. This design comes with several advantages, and particular in interest for the RoPax market is the reduction in speed loss and movements in head seas, which will help to keep schedules and increase the comfort level. The volume gained in the fore ship section may contribute to increased cargo carrying capacity, meaning additional lane meters and

a larger accommodation area. Due to the requirements these vessels meets, the study of this thesis will aim at establishing if this fore ship design could benefit from being adjusted from its original design, in order to meet the demands from this specific market.

With the increasing computational capacity, CFD is becoming more available as a design tool. By using CFD simulations, the X-Bow® and the modified design can be studied and evaluated considering the performance of the vessels. The impact on performance the modification has on the X-Bow®, can then be investigated. An illustration picture of a RoPax with an X-Bow® is shown in Figure 1.1.



Figure 1.1: RoPax with X-Bow® [1]

## 1.2 Motivation

The motivation behind this thesis originated from a research project from Ulstein Design and Solutions. The project was carried out in cooperation with the company, and will be beneficial for the company if notable differences between the original fore ship design and a modified design can be discovered by the use of CFD simulations. This study will aim at establishing if the original design could benefit from being adjusted to meet the demands of the RoPax market, and if CFD methods have the potential to capture the difference at design stage.

To achieve this, a procedure aiming at testing and comparing different designs with regard to some specific performance factors must be established. Some performance factors must be determined, and the original design must be modified aiming at improving these factors.
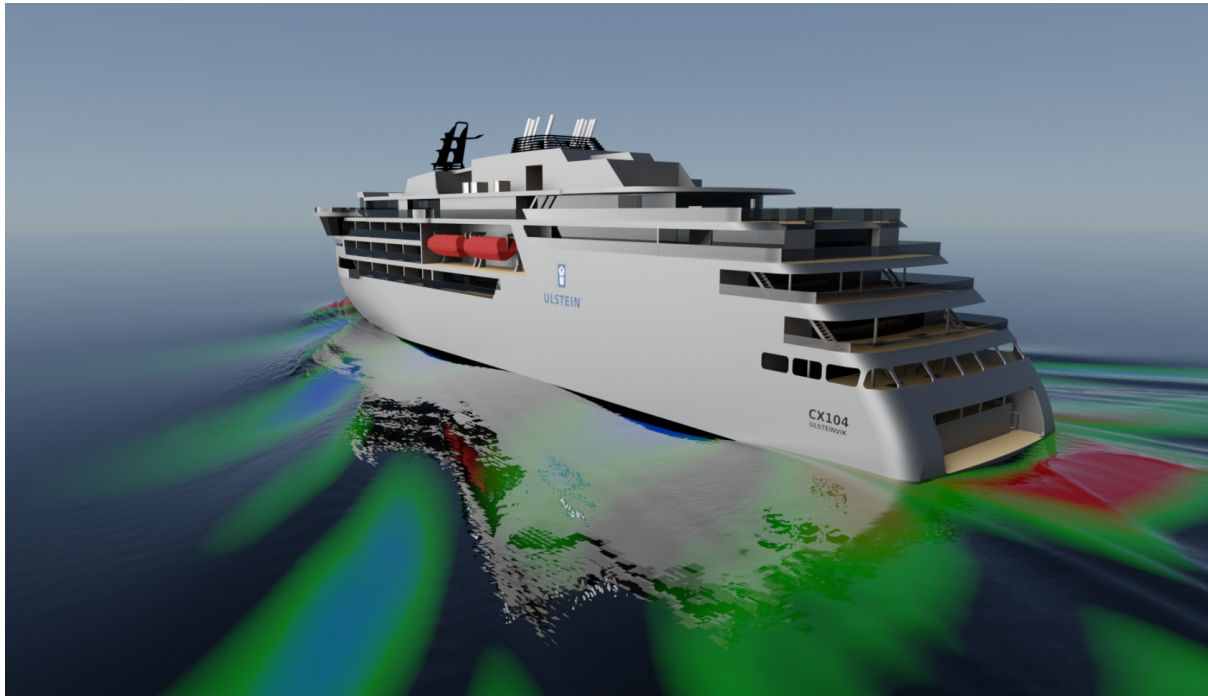
Figure 1.2: Typical Illustration of CFD Computations of a Passenger Vessel [2]

Due to confidentiality restrictions, the current study uses an approximation of an X-Bow®️ derived from pictures. The bow used as reference is therefore not an official X-Bow®️ that Ulstein would develop for commercial projects. However, Ulstein's hydrodynamic team has judged the volume distribution to be representative, and the reference bow to be suitable for a relative comparison of the performance of alternative designs as presented in this report. The results from the analysis could be used to evaluate if an adjustment of the original X-Bow®️ could be beneficial in order to meet the requirements from a new segment. Figure 1.2 shows an illustration of CFD computations for a cruise vessel from Ulstein.

## 1.3 Scope

The scope of the thesis will be within the boundaries of three topics, the key performance factors for a RoPax vessel, two different ship design solutions and CFD simulations to carry out the tests. This is illustrated in Figure 1.3.

To determine and rank key performance factors specific to a RoPax vessel is important to be able to evaluate if the design meets the demands for this market segment. To collect and evaluate every available performance factors would be an excessive amount for a project with a limited time schedule and resources. In order to complete a valuable evaluation but still narrow it down to a doable amount of work, factors like calm water resistance and ship accelerations in waves representative of a given trade route should be in focus.

Two different hull design should be developed, one baseline design, and one additional hull design combining the baseline design with an compatible existing technology. The design of the additional hull should be developed aiming at improving the performance of the vessel with regard to the derived performance factors.

To evaluate the designs with regard to these performance factors, CFD simulations will be used. The procedure of the CFD modeling should be well described. The CFD simulations will be performed using Star CCM+.
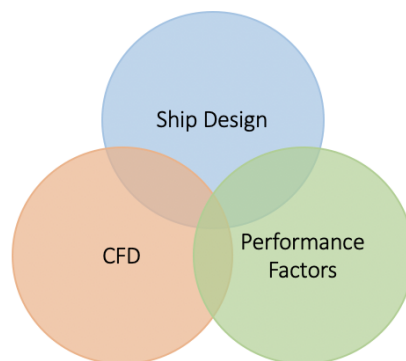


Figure 1.3: Scope

## 1.4 Objective and Research Questions

The main objective of this thesis is to document the process of a CFD model setup used to evaluate the modification of a hull design, and to use the results from the simulations to evaluate the impact this modification will have. The hull designs should be evaluated with regard to performance factors considering ship motions and efficiency in calm water and in waves representative for the North Sea region. To do this, relevant performance factors for a RoPax vessel should be discussed. These performance factors should be weighed to judge the evolution of the hull design along the project.

The shape of the original design will be representing an existing design, and should be the base of the additional hull design. Existing technologies that can be combined with the X-Bow® to further improve the hull performance in relation to the listed performance factors should also be discussed.

The CFD simulations should be carried out by using Simcenter Star CCM+, a simulation software developed by CD-Adapco. The output from the simulations should cover information that can be used to evaluate if the design combination of the baseline design and an existing technology could be beneficial for this operation. The research questions related to this objective was defined in cooperation with the supervisor at NTNU and the industrial collaborator. Answering and discussing the research questions will be in focus, and they are listed up below:

RQ 1: What are the relevant bow designs with respect to seaworthiness?

RQ 2: How can CFD simulations be used to assess seaworthiness?

RQ 3: How can performance increase be quantified?

# 1.5 Thesis Outline

**Chapter 1 - Introduction:**

In the first chapter, the problem statement is introduced, including motivation, scope and objective of the thesis. It also includes a discussion of research questions related to the thesis.

**Chapter 2 - Literature Review:**

The second chapter contains the current state of art for topics relevant for this study. This includes the X-Bow, Ship Performance and CFD.

**Chapter 3 - Methodology:**

The third chapter presents the methodology used this thesis, including the hull modification, CFD setup and Time Series analysis.

**Chapter 4 - Results and Discussion:**

**Chapter 5 - Conclusion and Future Work:**

# Chapter 2

# Literature Review

## 2.1 X-Bow®

The characteristic fore ship design X-Bow® is a converted bow concept that was developed by Ulstein Design and Solutions. The design was revealed in 2005, along with a contract of the anchor handling tug supply vessel *Bourbon Orca*, which is shown in Figure 2.1. More than 100 vessels with the X-Bow® are either under construction or operating around the world. The use has expanded into several segments, like the offshore renewables industry, expedition cruise and trawling [3]. The design has been regarded by the industry as a major milestone in the development of hull shapes for this sector.



Figure 2.1: Bourbon Orca [4]

Compared to a conventional bow design, this design is at its longest at the waterline, towards the extreme point of the vessel, and therefore its name. This gives a continuous sharp bow shape and more buoyancy in the fore ship section, which helps the vessel to cut through the waves and distribute the force more evenly across its surface. This may improve the overall stability and reduce speed loss and ship motions in poor weather conditions, and also reduce the ship resistance, leading to less fuel consumption. In addition, the volume distribution in the fore ship section will be smoother, and the hull water line will be more slender. With these characteristics, the ship will be more suited for harsh weather conditions, especially considering reduced slamming forces and accelerations, meaning reduced vibration and a higher comfort level [3]. Figure 2.2 shows a tank test comparison between an X-Bow and a conventional bow design.



Figure 2.2: Model Test Comparison X-Bow vs Conventional Bow [5]

With a hull design like this there comes several advantages that are interesting to investigate considering other vessel types. For a RoPax vessel, this means more volume in the fore ship section, which can be beneficial considering cargo carrying capacity and accommodation.

## Compatible Technologies

Several types of bulbous bows is a highly used technology considering ship performance. The principle behind the design and position of a bulbous bow is that the combination of the bow wave and the wave generated by the bulb results in a destructive interference, which again results in a reduced total wave making of the ship, as illustrated in Figure 2.3 [6]. The bulb parameters are essential, where the length of the bulb defines the phase of interference and the volume determines the width of the wave system [7].



▲ Only conventional bow   ▲ Only bulb (bulbous bow)   ▲ Conventional bow + bulb (bulbous bow)

The wave created by the bulb cancels that created by the conventional bow
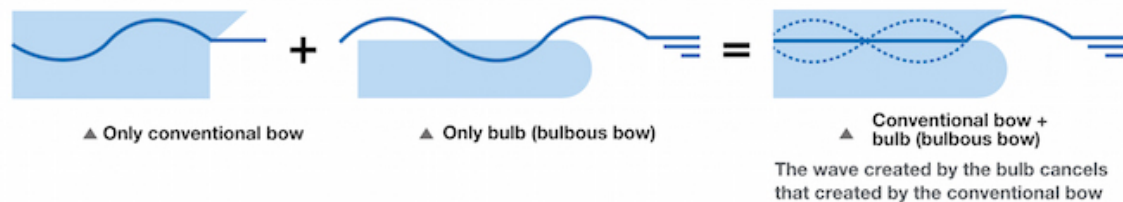
Figure 2.3: Influence of a Bulbous Bow [8]

Another advantage of a bulbous bow is the effect it has on the ships pitch motion. In many cases, the bulb is used as the fore-peak ballast tank, and when this is ballasted, it increases the weight at a larger distance from the Longitudinal Center of Gravity (LCG). This will increase the pitch radius of gyration, which helps increase the pitch period, which again results in less dynamic effect of the pitch motions.

In order to combine the inverted bow design with a bulbous bow, the shape and size of the bulb must be suitable for the mission of the ship. The interaction between the existing hull and the appendage must interact in a way that both of their advantages are kept, and the change must, at least in the first place, be moderate considering other important ship properties.

## 2.2 Performance Factors

The assessment of a vessels seakeeping abilities is based on the ships dynamic responses in the sea state and is related to some factors [9]:

- The main characteristics of the ship.

- The sea environment.

- How the ship encounter the environment.

- Requirements for seakeeping performance based on the vessels intended mission.
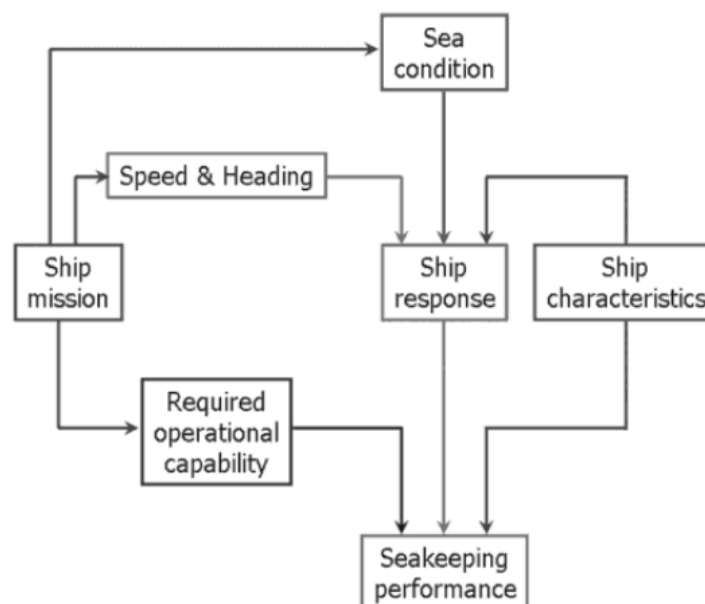


Figure 2.4: Seakeeping Performance Analysis [9]

The way these factors interact will determine the vessels seakeeping performance, which is illustrated in Figure 2.4. In order to evaluate rather the ships seakeeping abilities are sufficient regarding the operation area and mission, some key performance factors needs to be established. According to Volker Bertram [10], seakeeping of ships is investigated with respect to the following issues:

- Maximum velocity in a seaway, meaning involuntary speed loss due to added resistance in waves and voluntary speed reduction to avoid excessive motions.

- Route optimization to reduce total cost in form of fuel consumption and transport time.

- Structural design of ship with respect to loads in seaways.

- Comfort and safety for crew and passengers, such as motion sickness, danger of accidental falls or persons overboard.

- Ship safety; capsizing, large roll motions and accelerations, slamming, wave impact on superstructures or deck cargo, propeller racing resulting in excessive rpm for the engine.

- Operational limits.

The seakeeping abilities of a RoPax vessel are important to the integrity of the cargo and the comfort of crew and passengers [1]. In rough seas it is necessary to slow down in order to maintain safety and comfort, which is something that could challenge the ability of keeping schedules. Some of the key performance parameters for a RoPax vessel should therefore include ship resistance and ship motions, that should be evaluated in form of accelerations considering comfort and safety.

## Comfort Level

A ship at sea moves in six degrees of freedom, and these are illustrated in Figure 2.5. Surge, sway and heave are linear movements in the x, y and z direction. Roll, pitch and yaw are rotary movements about the x, y and z axis. Heave, roll and pitch can be oscillated at a natural frequency as they are subject to gravitational restoring forces, which is something that should be avoided.
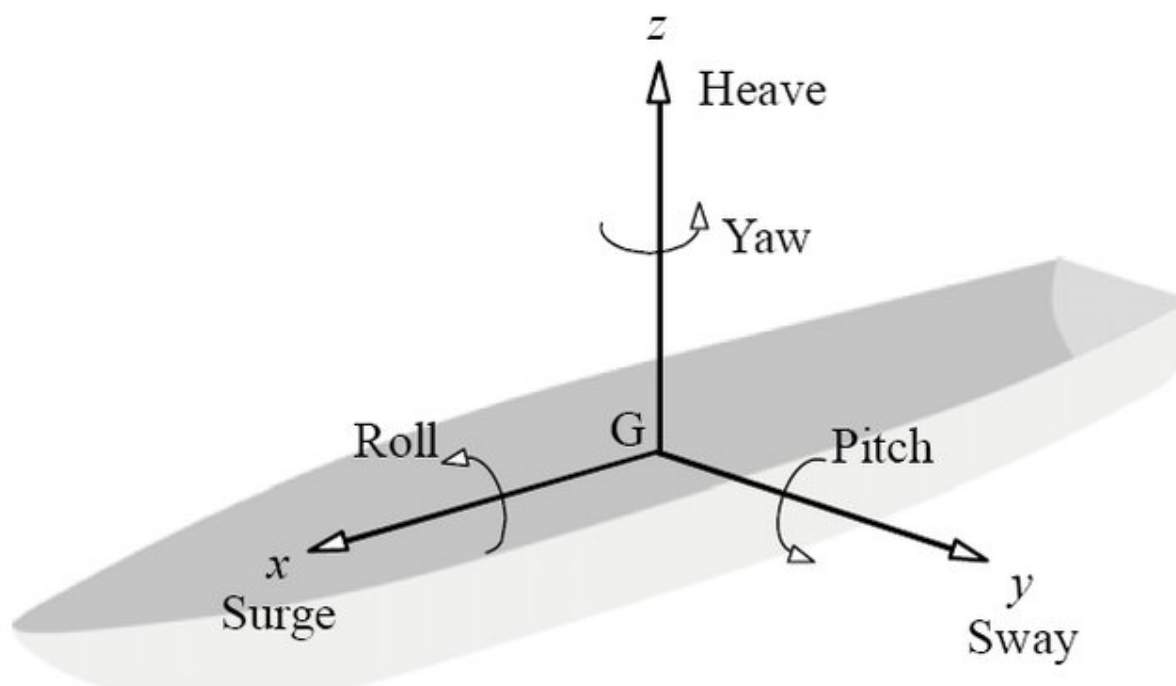


Figure 2.5: Ship Motions [11]

The comfort level on board a vessel is a broad term that needs to be narrowed down. In this study, the comfort level will be measured as the vertical acceleration in two different locations of the ship.

According to Nordforsk [12], there are a set of criteria regarding the level of comfort for crew and passengers on board different types of vessels. These criteria involves vertical and lateral accelerations, roll, slamming etc. and are highly relevant for the comfort level experienced on board. Due to several assumptions early in this project, such as for the Metacentric Height (GM), and also no specific location for the bridge, cabins etc., the comfort study for this thesis will not be an absolute comparison against international criteria, but a relative comparison between the two hull designs. The comfort study will also not include all factors necessary for a complete ship performance study considering comfort, but narrowed down to a set of factors suitable for the limited amount of time.

## 2.3 Computational Fluid Dynamics

Computational Fluid Dynamics (CFD) is the use of mathematics, numerical methods and computational softwares to simulate and describe fluid behavior and fluid flow. Computational power are used to simulate a fluids free stream flow, as well as the interactions of other fluids and objects [13]. Fluid flows can be described by partial differential equations, and in order to obtain an approximate solution numerically, it must be used a discretization method that approximates the differential equations by a system of algebraic equations, which can then be solved on a computer [14].

A fluid problem could be solved by knowing the physical properties of the fluid and using fluid mechanics to solve it. To describe these physical properties, mathematical equations like the Navier-Stokes (NS) equations can be used [15]. The NS equations are the fundamental basis of most CFD problems, and is therefore considered as the governing equations in CFD. These equations are based on three main principles; conservation of mass, conservation of momentum and conservation of energy. The NS equations for incompressible fluids are showed below, where equation 2.1 is the continuity equation and equation 2.2 is the momentum equation.

$$\nabla \cdot u = 0 \tag{2.1}$$

$$\underbrace{\left(\frac{\delta u}{\delta t}\right)}_{\text{Time derivative}} + \underbrace{((u \cdot \nabla)u)}_{\text{Convection}} = \underbrace{\left(-\frac{1}{\rho}\nabla p\right)}_{\text{Pressure gradient}} + \underbrace{(\nu \Delta u)}_{\text{Diffusion}} + \underbrace{\left(\frac{1}{\rho}f\right)}_{\text{Volume force}} \tag{2.2}$$

where $u$ is the velocity vector, $\rho$ is the density, $p$ is the scalar pressure, $\nu$ is the kinematic viscosity and $f$ is the volume force.

## Turbulence Modeling

The shear forces acting on the ship hull generates a rotation of the fluid particles close to the hull, which results in a turbulent flow. A ship has a high Reynolds number, approximately $10^8$, and to compute the flow around the ship, a turbulent solver must be used. The Reynolds Average Navier-Stokes (RANS) equations are therefore used to calculate the turbulent flow. The velocity and pressure can be split into a mean and a fluctuation part, which is shown in equation 2.3 and 2.4.

$$u_i = \overline{u_i} + u'_i \tag{2.3}$$

$$p = \overline{p} + p' \tag{2.4}$$

When applying the mean and fluctuation part to the NS equation, this results in the RANS equations, as equation 2.5 and 2.6 shows.

$$\overline{u_j} \frac{\delta \overline{u_i}}{\delta x_j} = 0 \tag{2.5}$$

$$\frac{\delta \overline{u_i}}{\delta t} + \frac{\delta}{\delta x_j} \left[ \overline{u_i u_j} + \overline{u'_i u'_j} \right] = -\frac{1}{\rho} \frac{\delta \overline{p}}{\delta x_i} + \nu \frac{\delta}{\delta x_j} \left[ \frac{\delta \overline{u_i}}{\delta x_j} + \frac{\delta \overline{u_j}}{\delta x_i} \right] \tag{2.6}$$

In order to determine the turbulent eddy viscosity, the two-equation realizable $k - \epsilon$ turbulence model is solved. This equation solves transport equations for the turbulent kinetic energy $k$ and the turbulent dissipation rate $\epsilon$. The realizable $k - \epsilon$ model differs from the standard model as it adds an additional transport equation for the turbulent dissipation rate $\epsilon$, that is derived from an exact equation for the transport of the mean square vorticity fluctuation [16]. The two-layer approach enables the model to be used with fine meshes that resolves the viscous sublayer. The computation is divided into two layers, where in the layer next to the wall, the turbulent dissipation rate, $\epsilon$, and the turbulent viscosity, $\mu_t$ are specified as functions of wall distance. The values of the dissipation rate are smoothly blended with the values computed from solving the transport equation far from the wall, and the equation for the turbulent kinetic energy is solved across the entire flow domain [17].

## Finite Volume Discretization

The Finite Volume Discretization Method (FVM) is a method that is used to solve the governing Partial Differential Equations (PDEs) by transforming the mathematical model into a system of algebraic equations. This is done by dividing the flow domain into a number of small control volumes or cells by a grid, and integrating the governing differential equations over these control volumes, as illustrated in Figure 2.6. Variable values are to be calculated in a computational node at the centroid of each control volume. To express the variable values at the surface of the control volumes in terms of the nodal values, an interpolation method is used. Surface and volume integrals are approximated by using quadrature formulas, and as a result, algebraic equations for every control volume is obtained, where a number of neighbor nodal values appear [14] [18]. This method can accommodate any type of grid, which makes it suitable for complex geometries.
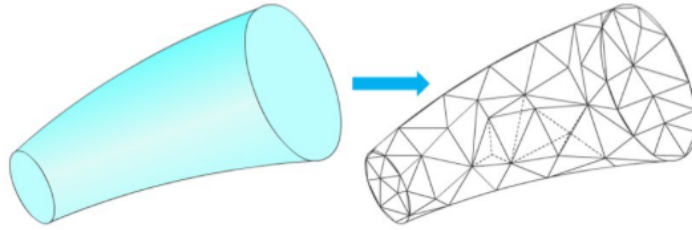


Figure 2.6: Finite Volume Discretization [19]

## Volume of Fluid Method

The ship is operating in both water and air, which makes the flow a multiphase flow. The Volume of Fluid method (VOF) is a simple multiphase model that predicts the distribution and movement of the interface of immiscible phases [20]. It is classified as an Euler method, meaning that it is described by a mesh that is either stationary or moving in a manner to accommodate the evolving shape of interface. With the VOF method, an additional scalar variable $\alpha \in [0, 1]$ represents the water-air ratio within a finite volume cell, as illustrated in Figure 2.7. To model the change of the free surface, a transport equation, as shown in equation 2.7, needs to be solved in addition to the NS equations.

$$\frac{\delta \alpha}{\delta t} + \nabla \cdot (\mathbf{u}\alpha) = 0 \tag{2.7}$$

The dynamic viscosity $\mu$ (eq. 2.8) and the density $\rho$ (eq. 2.9) is defined as a mix of the properties of the two respective fluids.

$$\mu = \alpha\mu_0 + (1 - \alpha)\mu_1 \tag{2.8}$$

$$\rho = \alpha\rho_0 + (1 - \alpha)\rho_1 \tag{2.9}$$



Figure 2.7: VOF Method [21]

## Time Step and Inner Iterations

**Time Step**

The Courant–Friedrichs–Lewy (CFL) number is one of the key parameters in CFD. The dimensionless number is dependent on the velocity, cell size and time-step, and is used to find an optimal ratio between these parameters. Equation 2.10 shows the formulation of the CFL number.

$$C = \frac{u\Delta t}{\Delta x} \tag{2.10}$$

where C is the dimensionless Courant number, $u$ is the magnitude of velocity, $\Delta t$ is the time step, and $\Delta x$ is the length interval.

The CFL condition indicates how the fluid moves through the computational cells within a time step. If CFL $\leq$ 1, the fluid moves from one cell to another cell each time step, but if CFL > 1, the fluid particles moves through two or more cells for every time step, which may effect the convergence of the solution in a negative way [22].

This gives a recommended CFL criteria of:

$$\Delta t < \frac{\Delta x}{u} \tag{2.11}$$

**Inner Iterations**

Within every time step, a number of iterations are solved. In a transient case, the governing equations are solved at each inner iteration. The number of inner iterations are dependent on the amount of change from each time step.

The implicit unsteady approach is a time integration scheme available for transient analysis. In the implicit unsteady approach, each time-step involves a number of inner iterations to converge the solution for the given time. If using the implicit unsteady approach, the user is required to set the physical time-step size, the CFL number and the number of inner iterations. This scheme calculates the involved equations both for the current and following state [23]. Compared to other methods, an implicit scheme requires more memory and are more complicated to use, but allows for larger time steps and better stability [14].

## Boundary Layer

An accurate prediction of flow and turbulence across the wall boundary layer is essential to obtain good results from the simulations. This can be obtained by either resolve the near-wall region all the way down to the wall, or by applying a wall function. Instead of resolving the viscous affected region, a wall function will bridge this region between the wall and the fully turbulent region [24]. The inner region of the boundary layer can be split into a viscous layer, which is closest to the wall and almost laminar, a log layer, which is equally dominated by viscous and turbulent effects, and a buffer layer, the layer in between. In the outer region the turbulent effects dominates the viscous effects. To define the extent of the sublayers, the non-dimensional $y^+$ value can be used. Figure 2.8 shows $u^+$, the non-dimensional velocity, as a function of $y^+$ across the boundary layer region.
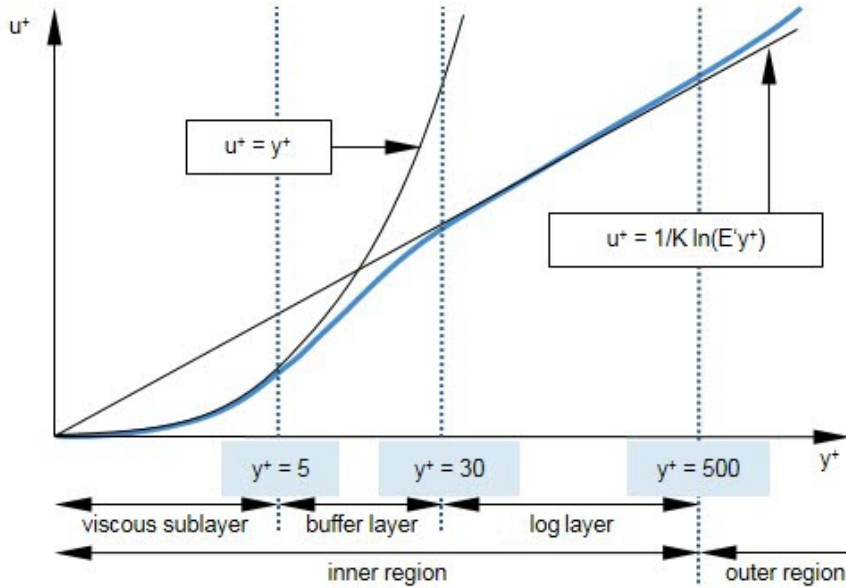


Figure 2.8: $y^+$ regions [20]

Equation 2.12 is used to define the height of the near wall cells,

$$y = \frac{y^+}{R_e \sqrt{\frac{C_f}{2}} L_{PP}} \tag{2.12}$$

where $y$ is the absolute wall distance, $R_e$ is the Reynolds number and $C_f$ is the friction coefficient.

## Boundary Conditions

To set the primary variables of a model, sufficient information is important. For the solver in Star CCM+ to know how the substance within the region and its environment interacts with each other, boundary and initial conditions are applied. A boundary condition can for example tell the solver that a certain amount of some substance are being added to the fluid domain and at which rate, or the pressure where substance are leaving the domain [20]. Initial conditions specifies the initial field data for the simulation, which affects both the convergence path and the required computational power. Examples of initial conditions are velocity, pressure, volume fraction and turbulence quantities. The boundary conditions used in this study are explained below.

### Velocity Inlet

A velocity inlet boundary is usually used as an inflow condition where the distributions of velocity and fluid properties must be known. The conditions are prescribed and used to calculate the fluxes of inlet volume, momentum and energy.

### Pressure Outlet

The pressure outlet boundary is an outflow condition, and the boundary pressure can be considered as the static pressure of the environment that the fluid enters.

### Symmetry Plane

A symmetry plane boundary represent an imaginary plane of symmetry in the simulation. In locations where the geometry and the flow are symmetric, the symmetry plane can be use to reduce the simulation runtime. This boundary can also be used as a slip wall, which means that there is no shear stress in the fluid.

### Wall

The wall boundary condition is used for surfaces that are not permeable. For this condition, a non-slip condition is added by default, meaning that the fluid will stick to the wall and move with the same velocity as the wall.

## Mesh Generation

A mesh can be defined as a discretized representation of the computational domain that the physics solvers use to provide a numerical solution [20]. A numerical grid divides the solution domain into a finite number of subdomains [14]. Star CCM+ offers several different meshing tools, and the ones that was used in this thesis are explained below.

- **Surface Remesher**: The surface remesher is a tool that can be used to retriangulate the surface. This is done to improve the overall quality of an existing surface. The properties of the surface remesher model can be changed during the meshing process in order to provide additional meshing control. In addition, when the prism mesher option is selected, the surface remesher aids the subsurface generator.

- **Automatic Surface Repair**: The automatic surface repair is a procedure for correcting geometric problems that can occur in the remeshed surface once the surface remeshing process is complete.

- **Trimmed Cell Mesher**: A trimmed cell mesher provides a robust and efficient method of producing a high-quality grid. It combines a number of highly desirable meshing attributes into one meshing scheme. This method can be used for both simple and more complex geometries and uses mostly hexahedral cells with minimal skewness. It also allows for user-defined refinement controls and alignment with a user specified coordinate system.

- **Prism Layer Mesher**: In order to improve the accuracy of the near wall flow, prism layers are necessary. A prism layer is defined by parameters like its thickness and the number and size distribution of prism cell layers.

- **Surface Control**: Surface controls can be used to further control the mesh on part surfaces, geometry parts and composite parts. One can modify several mesh controls, such as target and minimum surface size, prism layers and wake refinement. These values overrides the default control. Surface controls can be used to refine the mesh for a certain area, or to make the mesh coarser in areas far from the hull in order to make the simulation less computational demanding.

- **Volumetric Control**: Volumetric controls can be included to increase or decrease the mesh density locally. This tool can be applied to any combination of meshing models, and specific cell sizes withing the zone for each mesh generation stage can therefore be set.

## Convergence Criteria

Finally a convergence criteria for the iterative process must be set. There are usually two levels of iterations, inner iterations and outer iterations. The inner iterations handles the solving of the linear equations, and the outer iterations handles the non-linearity and coupling of the equations [14]. The decision of when to stop the iterative process is important considering both accuracy and efficiency.

## Motion Modeling Method

In general, motion can be defined as the change of position of a body with respect to a certain reference frame [20]. In transient simulations, mesh motion models allows the user to move the computational domains vertices during the simulation.

Morphing is a mesh method that displaces mesh vertices according to the motion of boundaries or regions. The morphing motion enables non-rigid motions of boundaries to simulate surfaces changing shape or location in the same simulation. This can for example be used to simulate the motion of an object where the boundaries are not changing shape, but the mesh vertices must morph in order to accommodate the movement [25]. Star CCM+ software provides a Dynamic Fluid Body Interaction (DFBI) Morphing motion, which is a variant of the morphing motion that is used for DFBI cases. The DFBI module is used to simulate the motion of a rigid body in response to forces. There are two types of rigid bodies, *Continuum Body* and *Mechanical body*. A continuum body is used for applications where the 6-DOF body is required to interact with a physics continuum in order to calculate the fluid forces and moments that is acting on the body, and is the one used for this thesis.

## Post Processing

Star CCM+ allows the user to post-process the solution after each iteration or time-step, both while the simulation is still running as well as when the simulation is complete. All data from the simulations are stored in field functions, and can be visualized by using reports, scenes and plots [20].

# Chapter 3

# Methodology

The main objective of this thesis is to set up a procedure to assess and compare two different hull designs with respect to resistance and seaworthiness by using CFD. This chapter describes the model setup for the resistance and motion study, including the applicable theory. This resolves research question 2 and 3, about how CFD simulations can be used to assess seaworthiness, and how performance increase can be quantified (ref. Chapter 1, Section 4).

The CFD simulations was divided into two parts. The first part was conducted in calm water to measure the resistance of the ships, and the vessels was fixed against rotation and translation. The other part of the simulations, which was the main part of the thesis, included incoming regular waves, and the ship was free to translate in z-direction and to rotate around the y-axis in order to measure the heave and pitch motions. This method was performed on both of the designs, and the results of these simulations was used to evaluate the presence of the bulb for this type of hull shape.

## 3.1 Hull Design

The original hull design in this study was representing a RoPax vessel with an X-Bow, but due to confidentiality it was not the original X-Bow. The original design will be referred to as *Design 1*, and the modified design will be referred to as *Design 2*.

The objective of this thesis was to compare two hull designs with regard to seaworthiness by using CFD simulations. As mentioned earlier, the term seaworthiness is a broad term that needed to be narrowed down. The main focus was then ship motions in head waves relevant for the North Sea region. The goal was to improve the design further with regard to the ship motions, but still keep the main benefits from Design 1. The designs was modeled in Siemens NX, and has the same main dimensions, which are described in Table 3.1.

Table 3.1: Hull Dimensions

| Parameter | Value | Unit |
|---|---|---|
| Length Between Perpendiculars (LPP) | 200.0 | m |
| Length Over All (LOA) | 215.0 | m |
| Width (B) | 28.0 | m |
| Draft (T) | 6.5 | m |
| Depth (D) | 23.0 | m |

### 3.1.1 Baseline Design

Design 1 is shown in Figure 3.1 and 3.2. This ships Block Coefficient (CB), which is the ratio of the underwater volume to a rectangular block with the same length, width and depth of the ship, was 0.629. The hull is at its longest at the waterline, which is one of the reasons to this designs hydrodynamic advantages. One of the main features of this design is the reduced hull resistance, an advantage that was tried to retain when modifying the design.
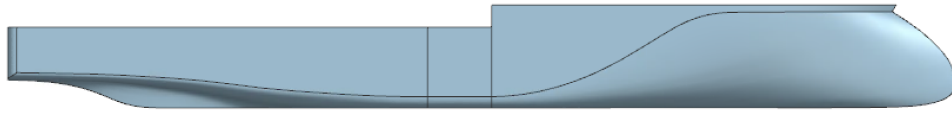
Figure 3.1: Design 1 - Profile View
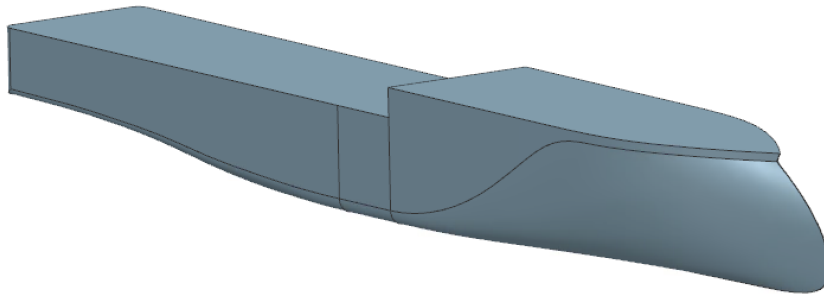
Figure 3.2: Design 1 - Front Right View

### 3.1.2   Modified Design

Design 1 was used as a base for Design 2, which is illustrated in Figure 3.3 and 3.4. The goal for this new design was to keep the main advantages from Design 1, but also to improve the ship motion capabilities by a slight change in the fore ship section. This design does also have an inverted bow shape, but compared to Design 1, it was also equipped with a bulbous bow shape. The volume change was moderate, it was only a slightly bit fuller in the fore ship section. The CB of this design was 0.631, and the location of the longitudinal center of gravity was a bit more forward than the original one. This hull was designed to keep the resistance characteristics of an inverted bow shape, but also to reduce ship motions by increasing the buoyancy in the fore ship section considering the integrity of the cargo and to increase the comfort level on board the ship.

Figure 3.3: Design 2 - Profile View
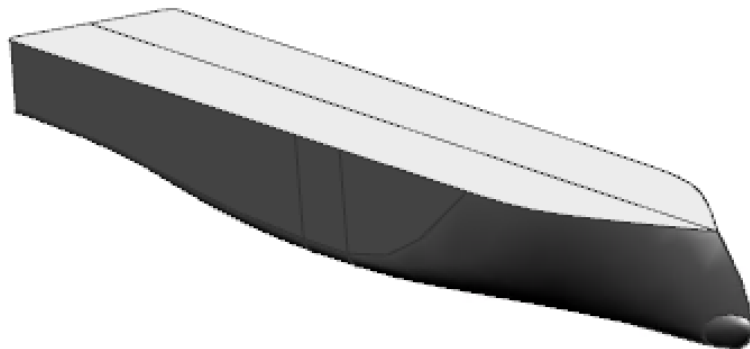
Figure 3.4: Design 2 - Front Right View

## 3.2 CFD Model Setup

The CFD simulations was carried out by using Simcenter Star CCM+, a complete multiphysics solution for simulations of products and designs operating under real world conditions. In this thesis, the mesh morphing method was used to resolve the problems that was involving moving and interacting components. In order to obtain comparable results, all simulations had the same environment configurations, including domain size, mesh size and initial conditions. The procedure of setting up the simulation models is described in this section.

### 3.2.1 Resources

The simulations was carried out on a virtual computer provided by NTNU, with a processor called Intel(R) Xeon(R) CPU E5-2690 v4 @2.60GHz and 20 GB memory. Product version STAR-CCM+ 12.04.011 (win64/intel16.3) was used and was processed on 8 cores.

### 3.2.2 Geometry Setup

The domain represents the surroundings around the hull, and the amount of surroundings included in the simulations is dependent on the size of the domain. The size of the domain was based on the length of the ship, and needed to be large enough to recreate a realistic image of the surroundings, but not unnecessary large as this would increase the required computational effort and memory. There had to be sufficient space in all directions in order to prevent the domain boundaries to affect the flow near the ship, in order to minimize the effect the location these boundaries have on the final solution. This was because the imposed flow needs to evolve properly from the inlet boundary ahead of the ship, and to prevent waves reflection from the exterior boundaries. The width of the domain was therefore preferred to be broad enough to not intersect with the Kelvin wake caused by the ship, and the outlet boundary often requires a damping zone to make sure no wave reflection occurs. The final dimensions of the domain is showed below.

$$\begin{bmatrix} x \\ y \\ z \end{bmatrix} = \begin{bmatrix} -3.0L_{PP}, & 2.0L_{PP} \\ 0.0L_{PP}, & 1.5L_{PP} \\ -1.0L_{PP}, & 0.5L_{PP} \end{bmatrix} = \begin{bmatrix} -600\ m & 400\ m \\ 0 & 300\ m \\ -200\ m & 100\ m \end{bmatrix}$$

The simulation was performed on a full scale ship in order to avoid any scaling errors as the scaling for the ship and for the waves is not in the same order and dimensions. Only half a domain was used considering a symmetry condition to make the simulation less computational demanding. The domain is illustrated in Figure 3.5 and 3.6.
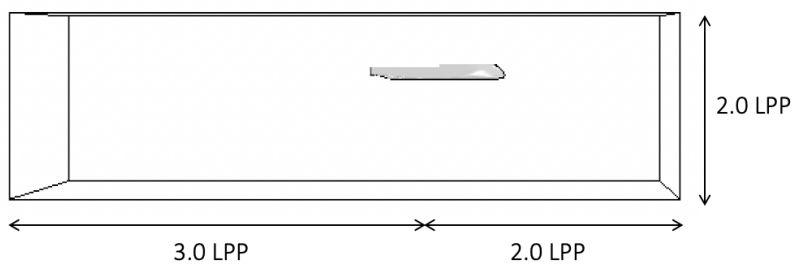
Figure 3.5: Domain Size
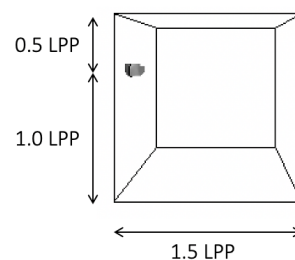
Figure 3.6: Domain Size

### 3.2.3   Boundary Conditions

To get a closed domain around the ship, each face of the domain was assigned a boundary condition to set constraints on the interior flow. The boundary conditions are shown in Table 3.2, and illustrated in Figure 3.7 and 3.8 :

Table 3.2: Boundary Condition Specifications

| Face of Domain | Boundary Condition |
|----------------|--------------------|
| Ship | Wall (No-Slip) |
| Inlet | Velocity inlet |
| Top | Velocity inlet |
| Bottom | Velocity inlet |
| Midplane | Symmetry plane |
| Side | Symmetry plane |
| Outlet | Pressure outlet |
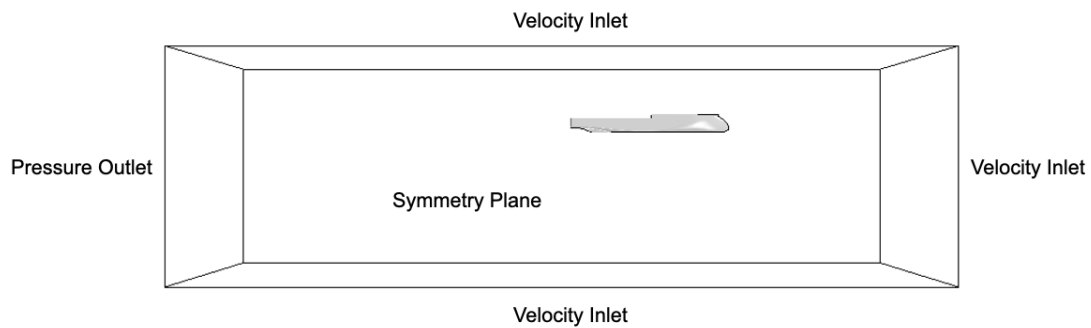


Figure 3.7: Boundary Conditions
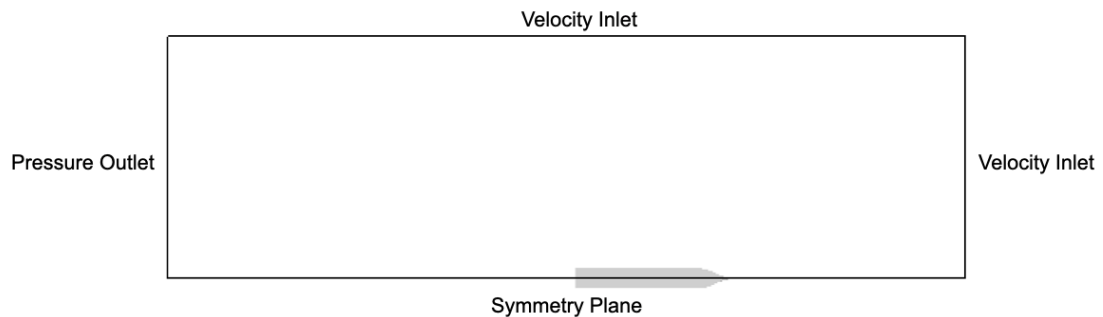


Figure 3.8: Boundary Conditions

### 3.2.4   Mesh Generation

For industrial use, simulations like these are processed on approximately 250 cores, compared to 8 cores that was available for this study. According to engineers at Ulstein, these resources reduces the necessities of several different refinement zones as the solver can handle a very fine mesh all over the computational domain. For a case with ship and wave parameters like in this, it would result in a mesh with approximately 20 million cells. Figure 3.9 to 3.12 is showing the mesh of the baseline design in a CFD model, generated from the CFD model from Ulstein.
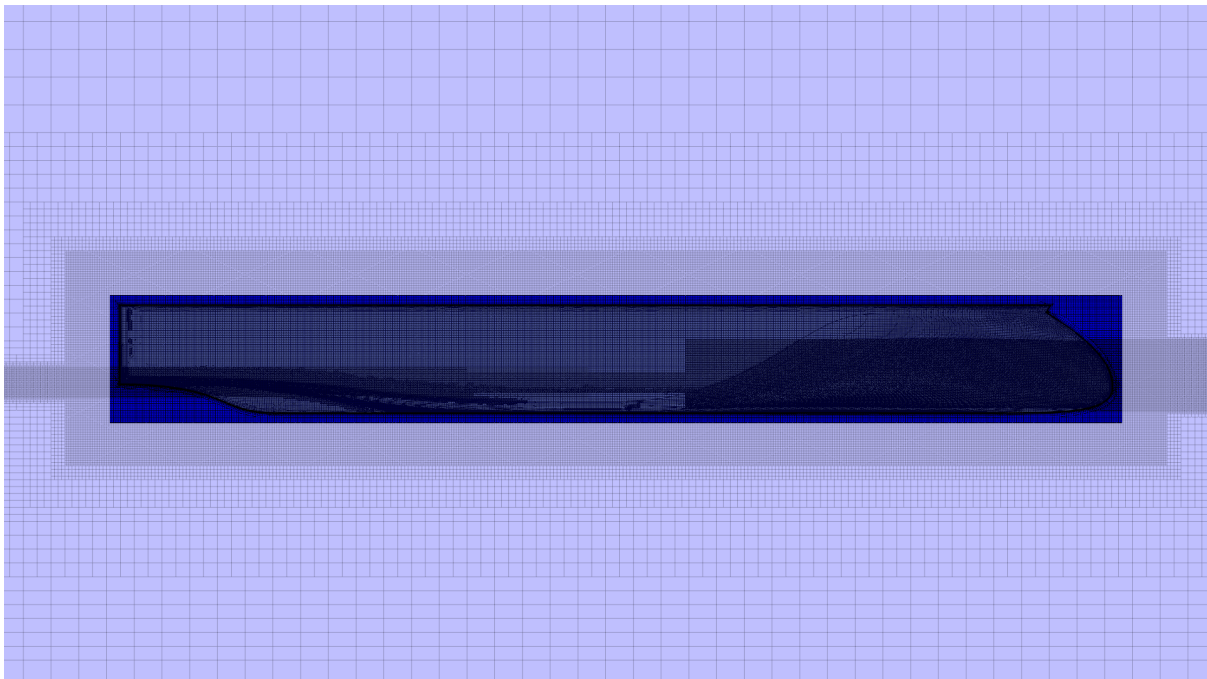


Figure 3.9: Hull Mesh
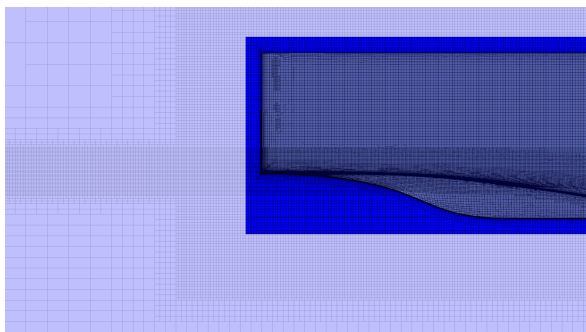


Figure 3.10: Stern Refinement
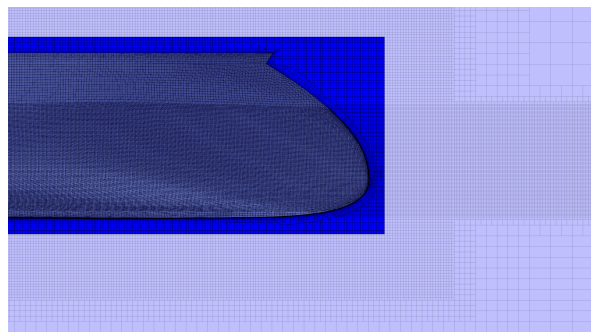
Figure 3.11: Bow Refinement
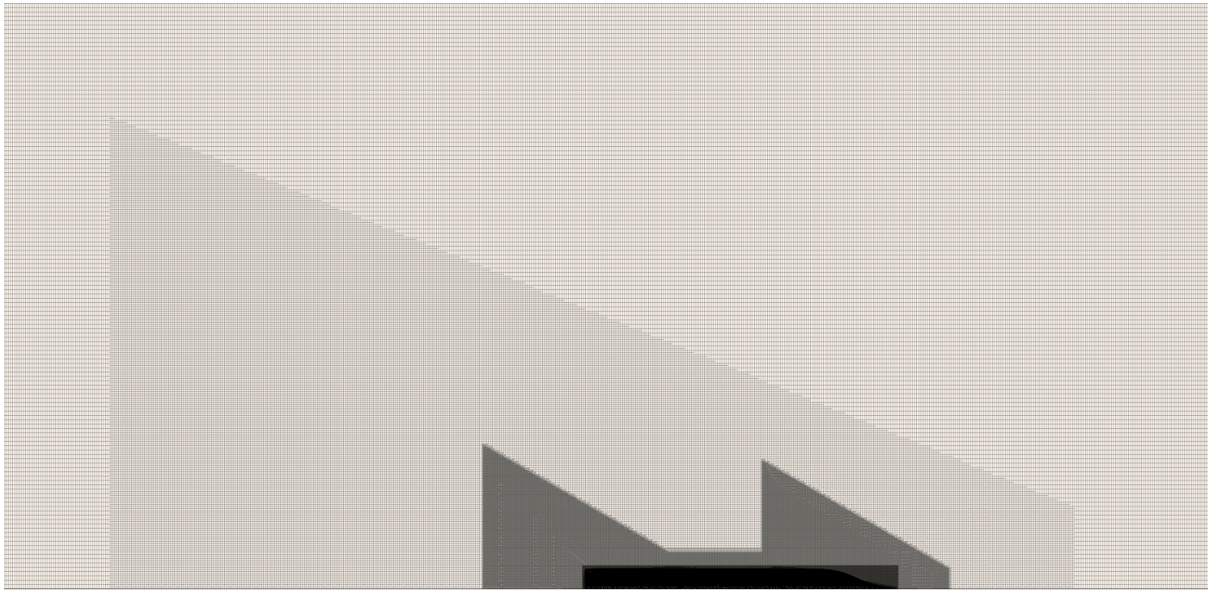
Figure 3.12: Hull Mesh Top View

To get usable results for this thesis, clever meshing considering a coarse base mesh with several refinement zones in forms of volumetric controls was necessary. This resulted in a mesh as fine as possible considering the available resources. To perform a mesh sensitivity study would therefore be meaningless. The mesh parameters and refinement zones was the same for both designs, and the final mesh had a total of approximately 600 000 cells for the full domain for both designs. An illustration of the mesh is shown in Figure 3.13.
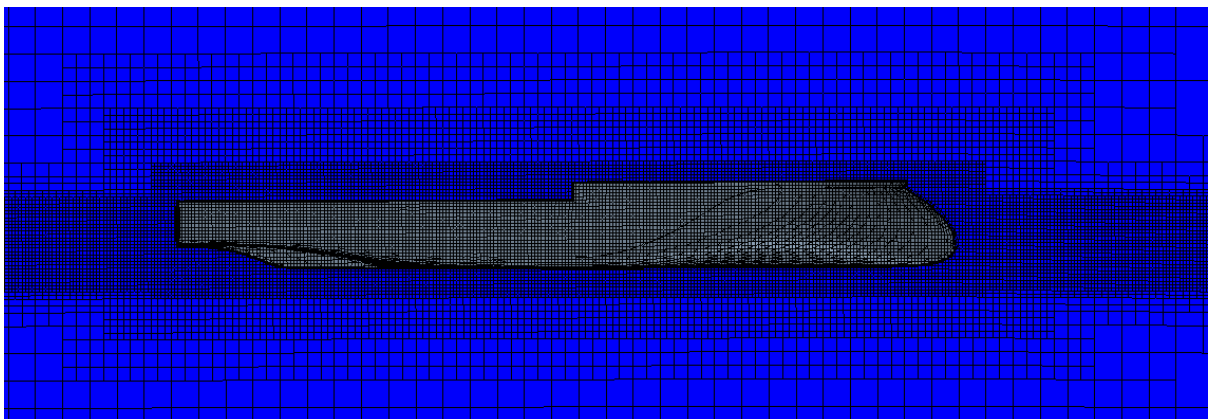


Figure 3.13: Full Domain Mesh

**Base Mesh**

Unless other was specified, the base mesh settings described the values that counts for the entire mesh. Table 3.3 shows the governing mesh settings. Figure 3.14 shows the full domain mesh, and 3.15 and 3.16 shows the mesh seen from above.

Table 3.3: Mesh Settings

| Parameter | Value | Unit |
|---|---|---|
| Base size | 30.0 | m |
| Target surface size | 50 | % |
| Minimum surface size | 5 | % |
| Surface curvature | 36 | pts/circle |
| Auto repair minimum proximity | 0.001 | - |
| Number of prism layers | 2 | - |
| Prism layer stretching | 1.5 | - |
| Prism layer total thickness | 0.5 | m |
| Volume growth rate | Medium | - |
| Maximum cell size | 1600 | % |
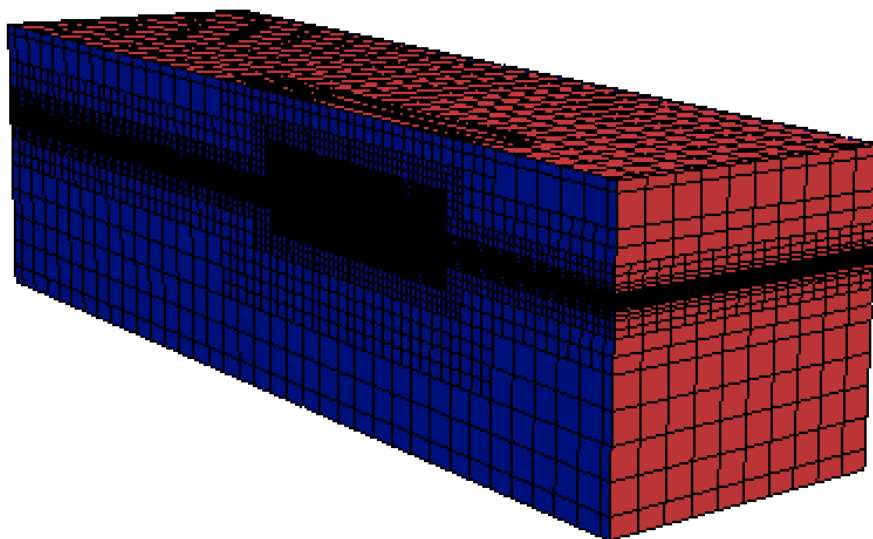


Figure 3.14: Domain Mesh
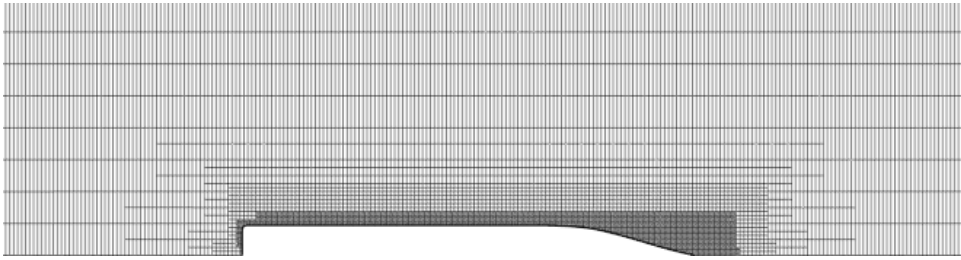
Figure 3.15: Top View of Full Domain Mesh
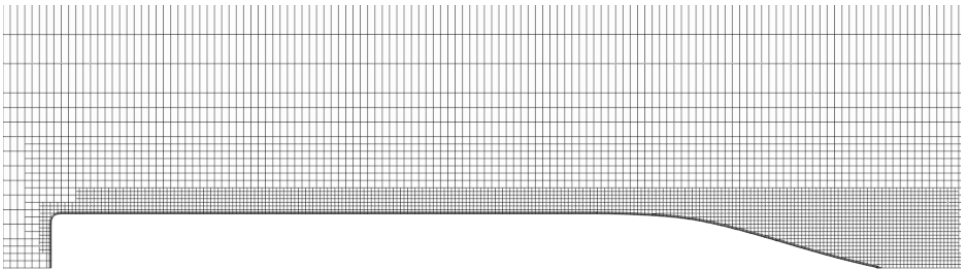


Figure 3.16: Top View of Full Domain Mesh

**Surface- and Volumetric Controls**

A surface control was added on the hull surface in order to ensure the prism layer settings and to get a finer resolution of the hull, especially important in the fore ship section. The surface size was set to 3 % of the base size.

With a coarse base mesh, two types of volumetric controls was used. Boxes was used for the mesh around the hull, and flat boxes was used throughout the whole domain in the free surface area to ensure a good resolution of the surface waves. Close to the hull, three levels of refinement was applied, and the cell size was isotropic dependent on the base size. Three refinement levels was applied also for the free surface area, but to reduce the amount of cells, the refinement was anisotropic, mostly refined in the z-direction. The extension of the free surface refinement in z-direction was large enough to cover the typical wave height in this study. The control volumes was overlapping each other, which resulted in a smooth transition from a fine to a coarser mesh. The cell size in the refinement zones are shown in Table 3.4 and 3.5, and is given in percentage of the base cell size. For every refinement zone, the grow rate was set to 1.3. The refinement zones are illustrated in Appendix A.

Table 3.4: Refinement zones around the hull

| Refinement Zone | Refinement Value |
|:---:|:---:|
| Hull Fine | 5% |
| Hull Middle | 10% |
| Hull Coarse | 30% |

Table 3.5: Refinement zones for the free surface

| Refinement Zone | X | Y | Z |
|:---:|:---:|:---:|:---:|
| Free Surface Fine | 5% | 50% | 3% |
| Free Surface Middle | 10 % | 50% | 5% |
| Free Surface Coarse | - | - | 30 % |

## 3.3 Ship Resistance

The study of ship resistance was conducted in calm water. To simulate the fluid flow, a flat VOF wave was used. This represents a calm plane of water, and both the current and wind was set to 6 m/s in x-direction, representing the ship velocity. To measure the ship resistance, the shear and pressure force in x-direction was monitored. The recommended run time on these types of simulations depends on when the solution converges and the force flatten out.

Figure 3.17 shows the pressure distribution on Design 1 during the resistance simulation, and Figure 3.18 shows the wave pattern for the same simulation.
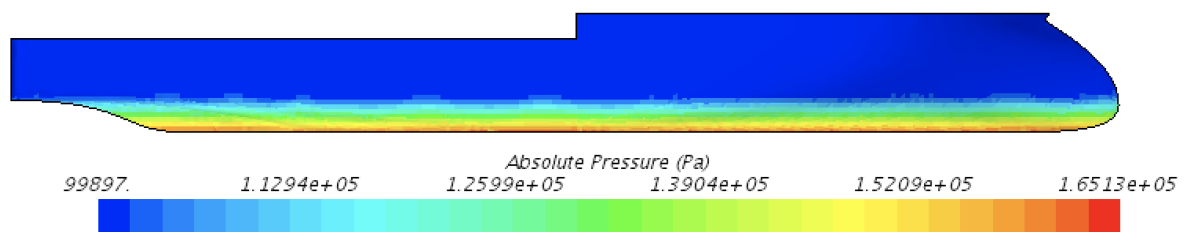


Figure 3.17: Absolute Pressure on Hull 1
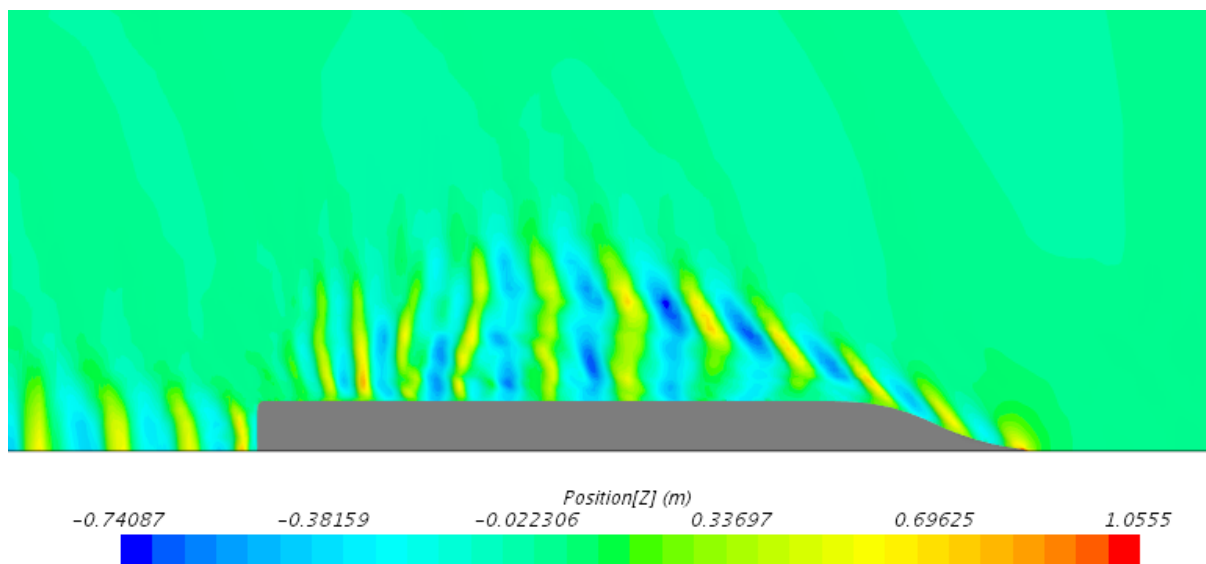


Figure 3.18: Resistance Ship 1

## 3.4 Ship Motions

The ship motion study was conducted with the same conditions as for the resistance study, but instead of a fixed ship, the ship was free to translate in z-direction and free to rotate around the y axis. For the most accurate modeling of regular waves as possible, a fifth order VOF wave with a velocity of 6 m/s was added. This wave velocity was applied as the wind and current velocity. The velocity of the current lead to some short length waves, which is something that might disturb the regular waves, and is visible in Figure 3.19. This appeared on the visual plots, but not in the time series, and was therefore disregarded. The waves propagate inside the domain from the inlet boundary condition, and was released at the same time as the simulation started. At the outlet of the domain, an artificial damping zone was used. The damping zone was dependent on the wave length, and was in this case set to 215 meters.
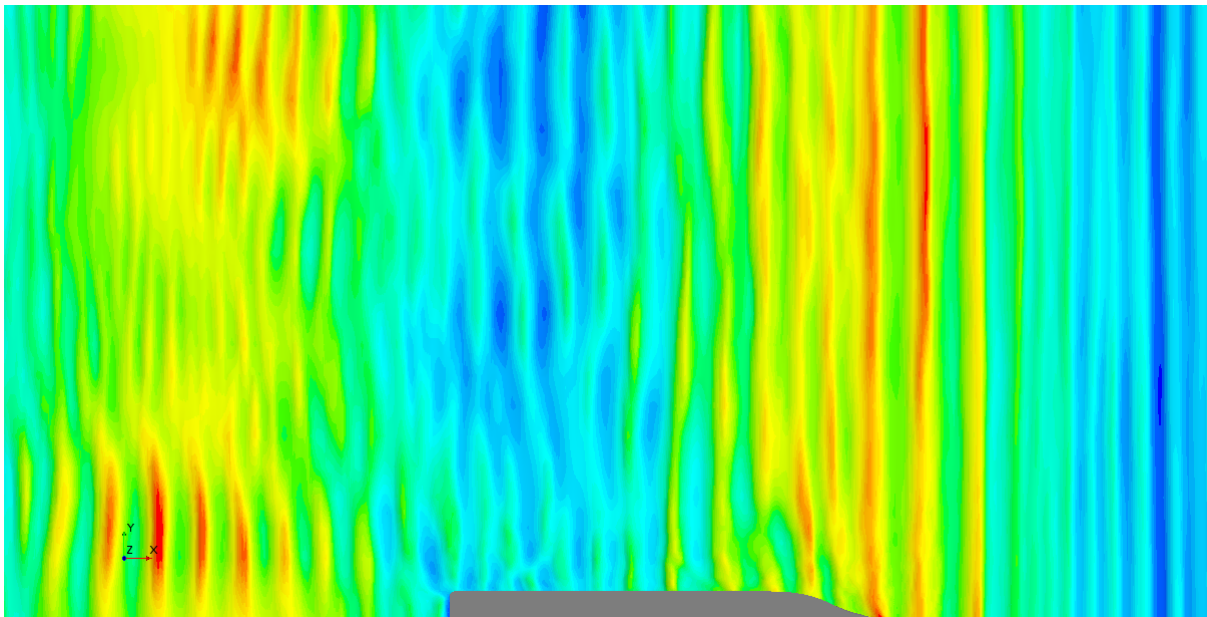


Figure 3.19: Water Surface

## Dynamic Fluid Body Interaction

To simulate the ship motion, a relevant DFBI motion object needed to be created. For this simulation, the DFBI Morphing method was used. The simulation started with a fixed ship, and after one physical simulation second, the ship started to get released. After five seconds the entire ship mass was released and the ship hull could move freely in heave and pitch direction. Figure 3.20, 3.21 and 3.22 shows how the mesh vertices moves to accommodate the movement of the ship.
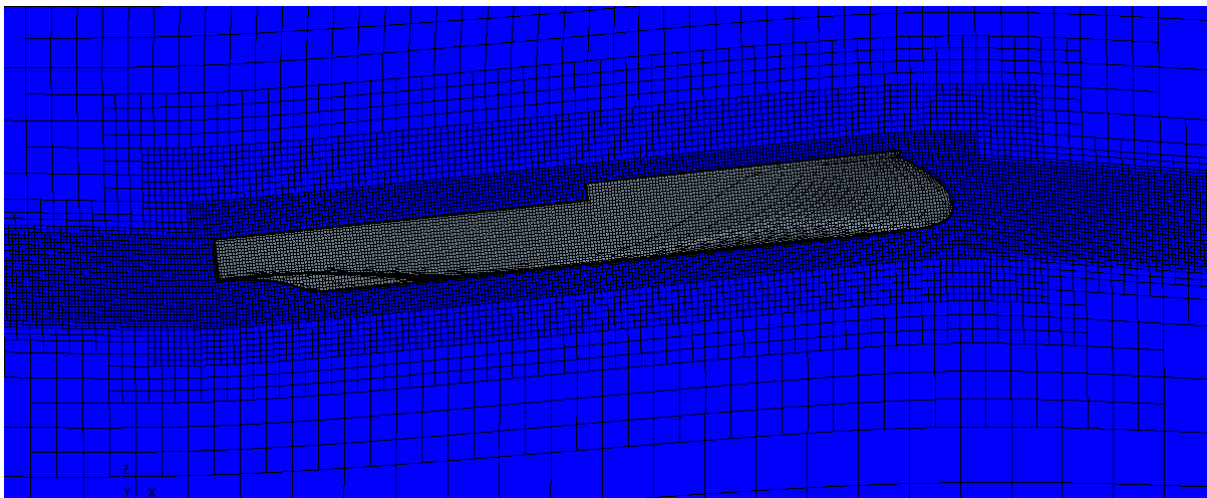
Figure 3.20: Mesh Morphing
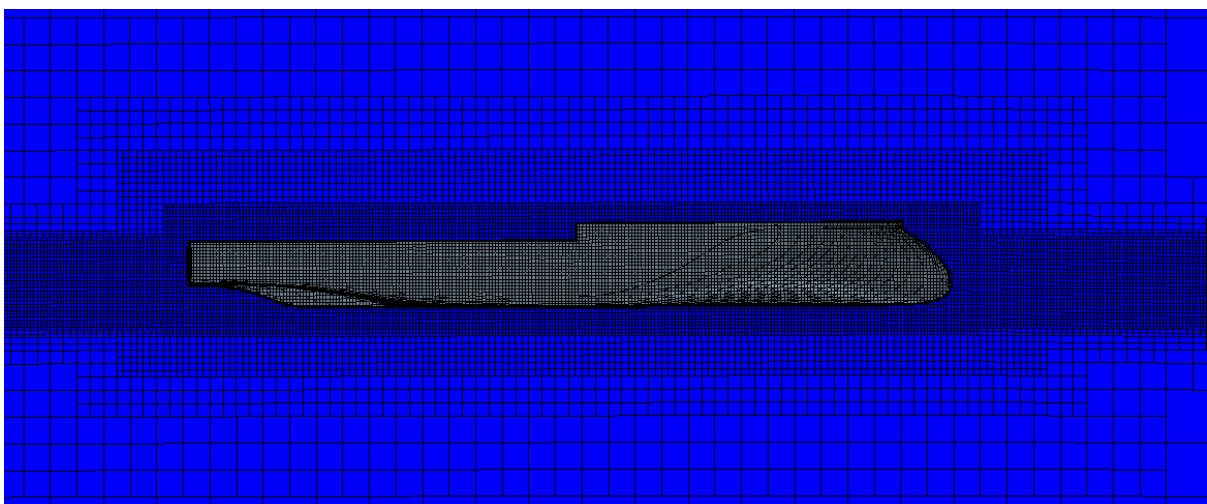
Figure 3.21: Mesh Morphing
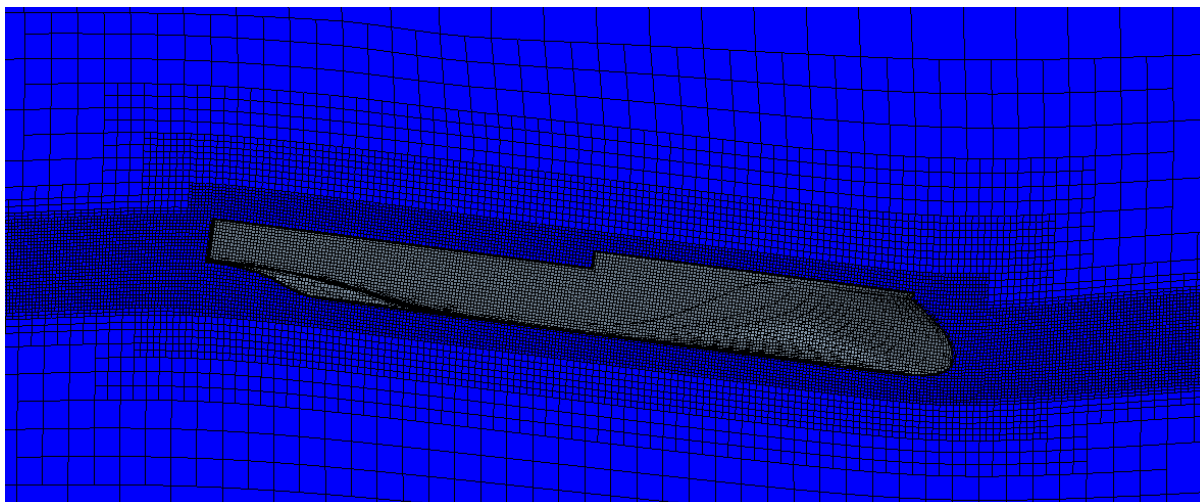
Figure 3.22: Mesh Morphing

Both ships was tested for six different wave conditions, including different wave lengths and wave heights. The wave lengths was chosen based on the length of the ship, and the wave height was based on typical wave heights for the North Sea. In addition, one extreme wave condition was chosen to test the wave characteristics of the inverted bow shape in higher and steeper waves. The wave conditions are shown in Table 3.6.

Table 3.6: Wave Conditions

| Wave Length | Wave Height |
|:---:|:---:|
| 215.0 m | 3.0 m |
| 320.0 m | 3.0 m |
| 140.0 m | 3.0 m |
| 105.0 m | 3.0 m |
| 215.0 m | 6.0 m |
| 200.0 m | 20.0 m |

## 3.5   Time Series Analysis

To evaluate the resistance and comfort level on board the vessels, necessary variables was obtained in time series. The ship resistance was measured as the shear and pressure force in x-direction, while heave and pitch was monitored as the motion experienced in the center of gravity. The time series shows the change of pressure and motion through the entire run.

For every wave condition, the simulation was ran long enough for the time series to give clear and constant results, at least until 15-20 pitch peaks was reached. In order to get this amount of pitch peaks for every simulation, the phase velocity of the longest wave was calculated. The phase velocity $c$ of a linear gravity wave with a wave number $k$ is given by

$$c = \sqrt{\frac{g}{k}} \tag{3.1}$$

where:

$$k = \frac{2\pi}{L} \tag{3.2}$$

The longest wave in this study was a 320 meter wave, so for this wave and with a velocity of 6 m/s, one can find:

$$c = \sqrt{\frac{9.81 * 320}{2\pi}} = 22.35 \tag{3.3}$$

$$22.35 + 6 \ m/s = 28.35 \ m/s \tag{3.4}$$

$$\frac{320}{28.35} = 11.28 \ s \tag{3.5}$$

There will be 11.28 seconds between each pitch peak, which means that in order to obtain the minimum of 15 peaks, the simulation must be running for at least 170 seconds. To be within these requirements, the simulations was ran for 200 physical seconds.

To handle the data from Star CCM+, Matlab and Python was used. Star CCM+ monitored the heave and pitch motion for every time step in the ships center of gravity. The center of rotation was assumed to be equal to the center of gravity, and based on this, the vertical motion in the center of rotation was found. This was also done for a position more exposed to ship motions, 100 meters forward from the center of rotation. This position was in the bow section where people do not normally stay, and considering comfort for passengers and crew there might be other locations that would be more interesting to investigate, such as the bridge, cabins, restaurants etc. But as there was no General Arrangement for the ships, these locations was unknown, and as the pitch motions was at its largest at this location in the bow section, it was considered conservative as one can be sure that the pitch motions will not exceed this value any other place on the ship. Figure 3.23 and 3.24 shows the two locations that was studied.
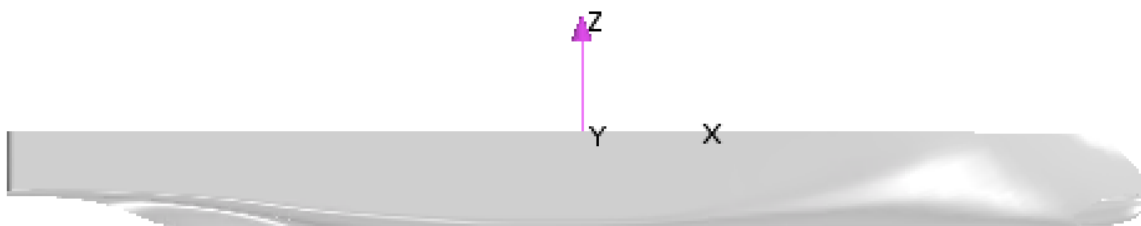
Figure 3.23: Center of Rotation

Figure 3.24: Second Control Point

## 3.5.1 Data Handling

The raw data from Star CCM+ was affected by noise due to vibrations and hydrody-namical disturbance, and some of the time series also had various time-steps throughout the simulation. This would affect the following calculations, so in order to avoid any following errors, the data needed to be resampled to a common time step and smoothed out by interpolation. This was done by using Python, and was done before combining the heave and pitch time series and deriving the combined equation. After handling the raw data from Star CCM+, the time series was used to find the vertical acceleration. The vertical motion in a specific point is a function of the combination of the heave and pitch motions, and was found by equation 3.6 and 3.7:

$$\eta = \eta_{3_{CoG}} + sin(\theta_{CoG}) \tag{3.6}$$

$$\eta = \eta_{3_{CoG}} + x * sin(\theta_{CoG}) \tag{3.7}$$

where $x$ is the distance from center of gravity to the specified location. From the vertical motion, the vertical velocity and acceleration was found by the time derivative as equation 3.8 and 3.9 shows:

$$\dot{\eta} = \eta_3 + x\eta_5 \tag{3.8}$$

$$\ddot{\eta} = \eta_3 + x\eta_5 \tag{3.9}$$

where $\eta_3$ is the heave motion, $\eta_5$ is the pitch motion, and $x$ is the distance from the center of gravity.

Figure 3.25 shows how the heave acceleration looked like without any smoothing of the time series, and Figure 3.26 shows the results from the same simulation after applying the smoothing.
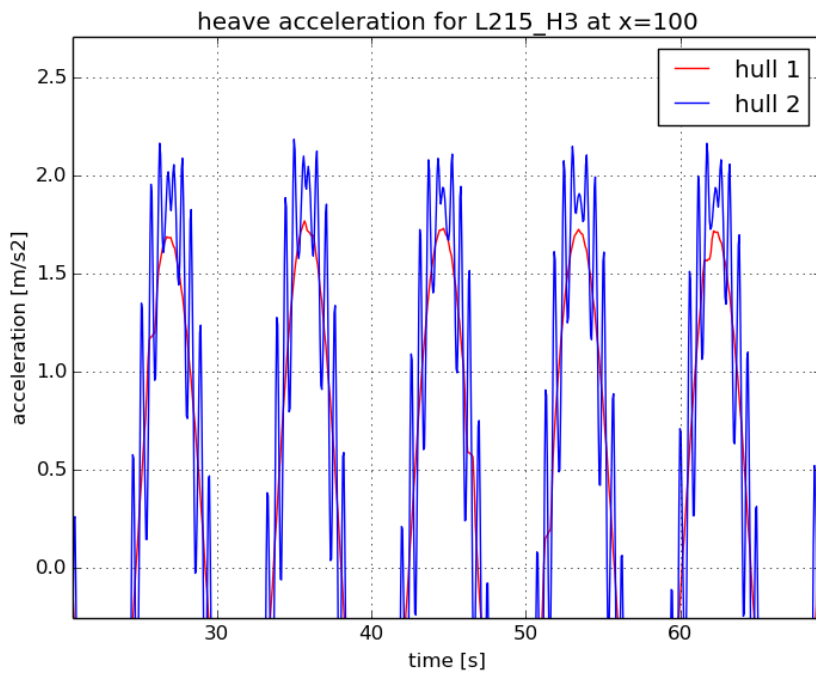
Figure 3.25: Measured Data
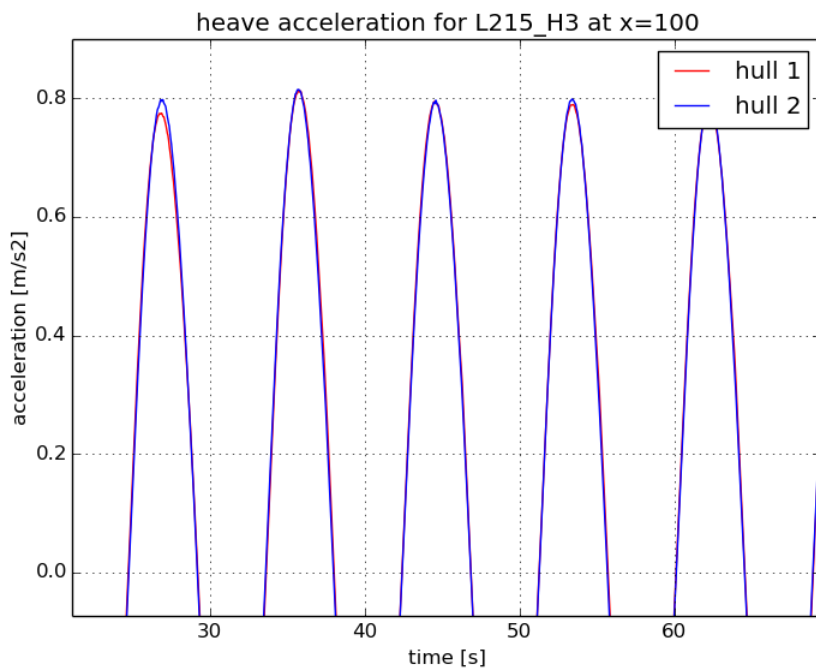


Figure 3.26: Smoothed Data

# Chapter 4

# Results and Discussion

The simulations was conducted based on the methodology explained in the previous chapter. This resulted in a calm water resistance study, and 12 different simulations measuring ship motions. Considering the ship motions study, the final results did not show any clear variations in most of the wave cases. Therefore, only some samples of the results are presented in this chapter, and the rest is to be found in the Appendix.

The presented results are images obtained from Star CCM+, and plots where the data from Star CCM+ are handled either in Matlab or in Python.

## 4.1 Hull Designs

Figure 4.1 shows the top view of the fore ship section of the original hull design, and Figure 4.2 shows the fore ship section of the modified design. The modified design still has a sharp shape, but is also equipped with a bulbous bow. This bulbous bow is also clear in Figure 4.3 and 4.4, which shows the front view of the two designs.
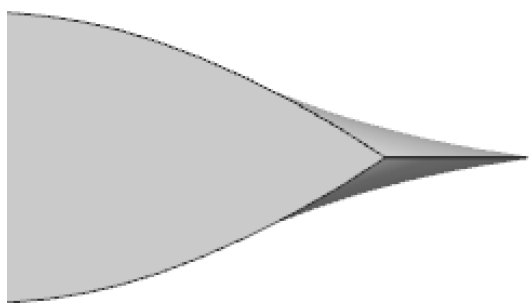


Figure 4.1: Top View Hull 1
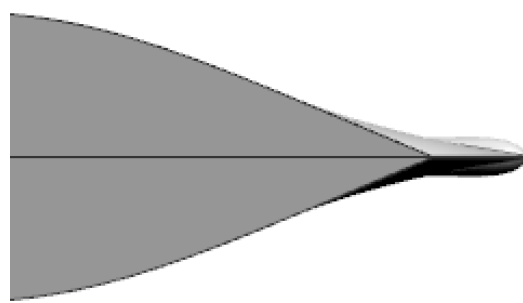


Figure 4.2: Top View Hull 2
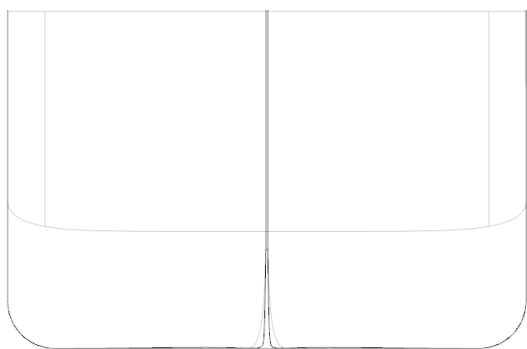


Figure 4.3: Front View Hull 1
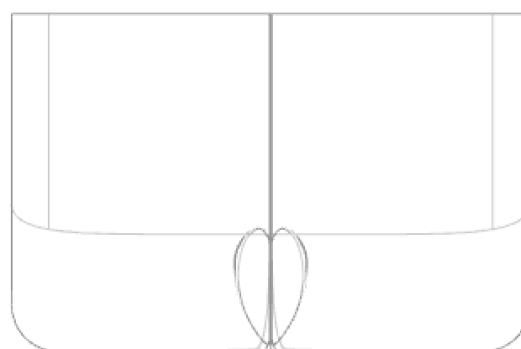


Figure 4.4: Front View Hull 2

A design change like this would affect other important ship properties, such as the displacement, the stability and the center of buoyancy. To change these parameters too much could therefore lead to severe consequences, which is why the design change was moderate. If a more drastic change should have been made, more analysis of the hull would have been necessary, and this was not prioritized in this study.

Table 4.1 shows some of the main parameters for the two designs. As mentioned earlier, the main dimensions of the hulls was similar, but the added volume in the fore ship section increases some of the ship parameters. As the figures and the table shows, the small volume change affects some ship properties in a small manner.

Table 4.1: Ship Hulls Comparison

| Parameter | Hull 1 | Hull 2 |
|---|---|---|
| Length Between Perpendiculars | 200 $m$ | 200 $m$ |
| Beam | 27.80 $m$ | 27.80 $m$ |
| Draft | 6.50 $m$ | 6.50 $m$ |
| Waterline Length | 214.44 $m$ | 214.44 $m$ |
| Volume | 22 751 $m^3$ | 22 802 $m^3$ |
| Block Coefficient | 0.6295 | 0.6309 |
| Prismatic Coefficient | 0.6390 | 0.6405 |
| Center of Buoyancy (rel. to Lpp/2) | -4.290 % | -4.174 % |
| Transverse metacentric radius | 12.20 $m$ | 12.17 $m$ |
| Centre of buoyancy above BL | 3.61 $m$ | 3.61 $m$ |
| Transverse metacentre above BL | 15.80 $m$ | 15.78 $m$ |

## 4.2 Calm Water Resistance

The calm water resistance comparisons was conducted with a ship velocity of 6 m/s. The simulations ran until the force converged, and was in this case running for 55 seconds. This is not a long time for a full scale simulation, but as the resistance calculations was not the main objective of the thesis, it was reasonable to stop the simulation after the force converged. Figure 4.5 and 4.6 shows the wave pattern generated with a ship velocity of 6 m/s.
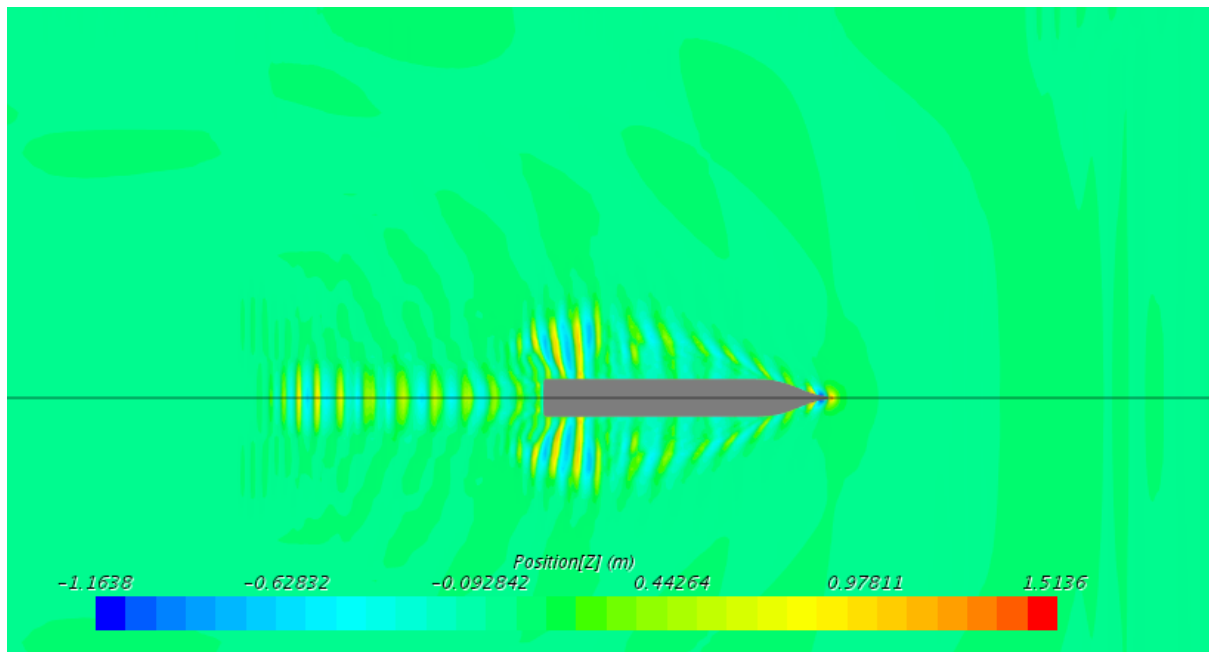


Figure 4.5: Wave Pattern Hull 1
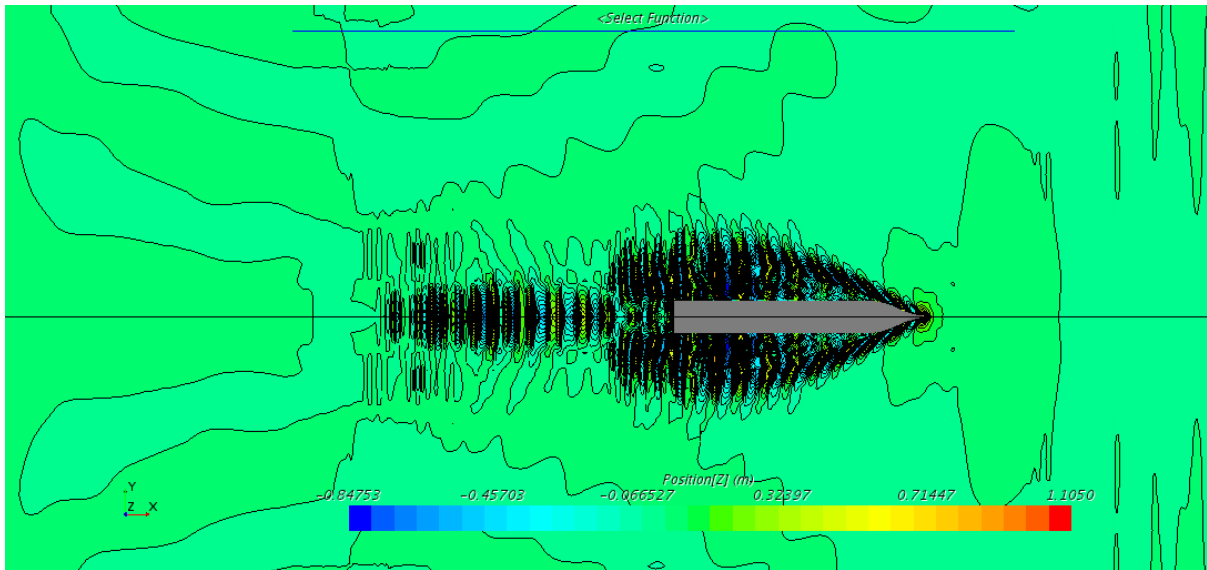
Figure 4.6: Wave Pattern Hull 1

Figure 4.7 and Figure 4.8 shows a plot of the pressure force and the shear force comparison for the two designs. Figure 4.9 shows a plot of the total force acting on the hulls, combining the pressure and shear force. The red line represents the original hull design and the blue line represents the modified design. The plots shows that there was an increase of the total force for the modified hull. The ship resistance is an important part of the ship performance, but it was not realistic and not the objective to create a design with less resistance than the original design in this study. The calm water resistance for both vessels are also showed in Table 4.2.
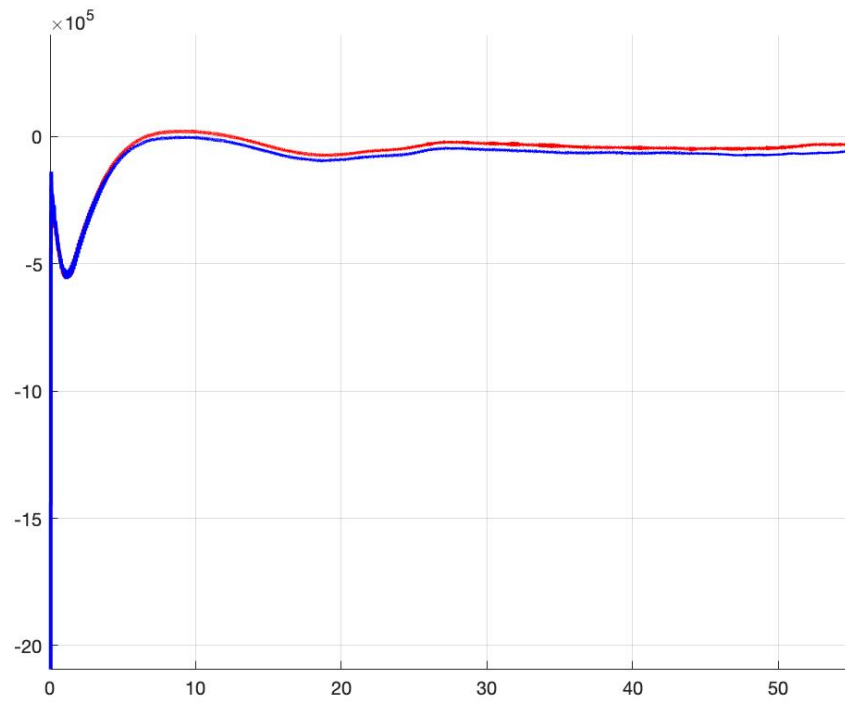
Figure 4.7: Pressure Force
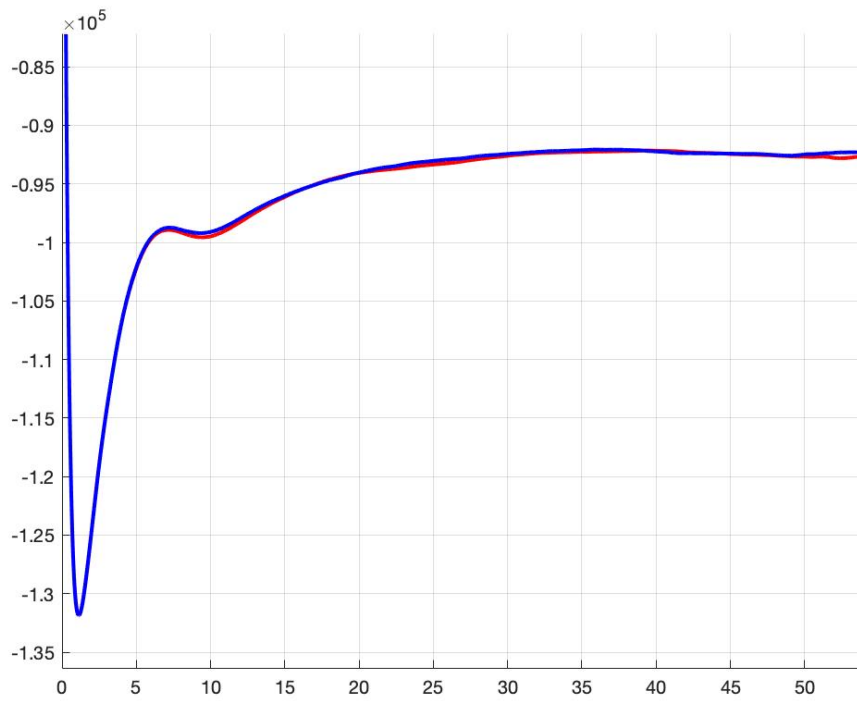


Figure 4.8: Shear Force
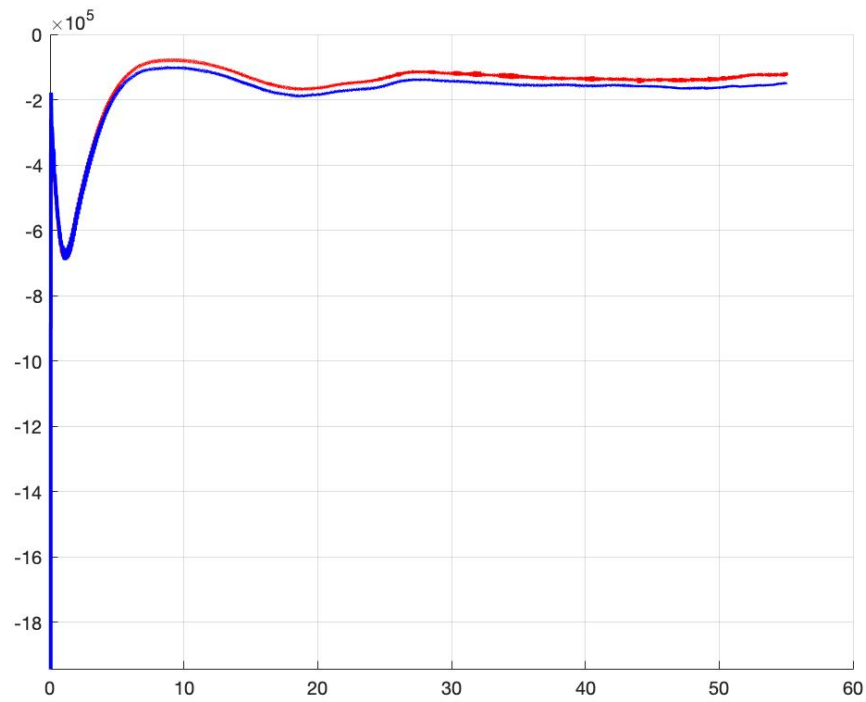
Figure 4.9: Pressure + Shear

Table 4.2: Calm Water Resistance

|  | Pressure [kN] | Shear [kN] | Net [kN] |
|---|---|---|---|
| **Hull 1** | 32.9 | 92.7 | 125.67 |
| **Hull 2** | 55.9 | 92.3 | 148.21 |

## 4.3 Ship Motions

The ship motion study required a DFBI motion method. This was a time consuming process where a set of different methods was tried, but did not provide stable results. Finally, the DFBI Morphing Method was chosen as this method provided stable and usable results. Every wave case was simulated for 200 seconds in physical simulation time. Figure 4.10 shows Design 1 in a wave simulation.
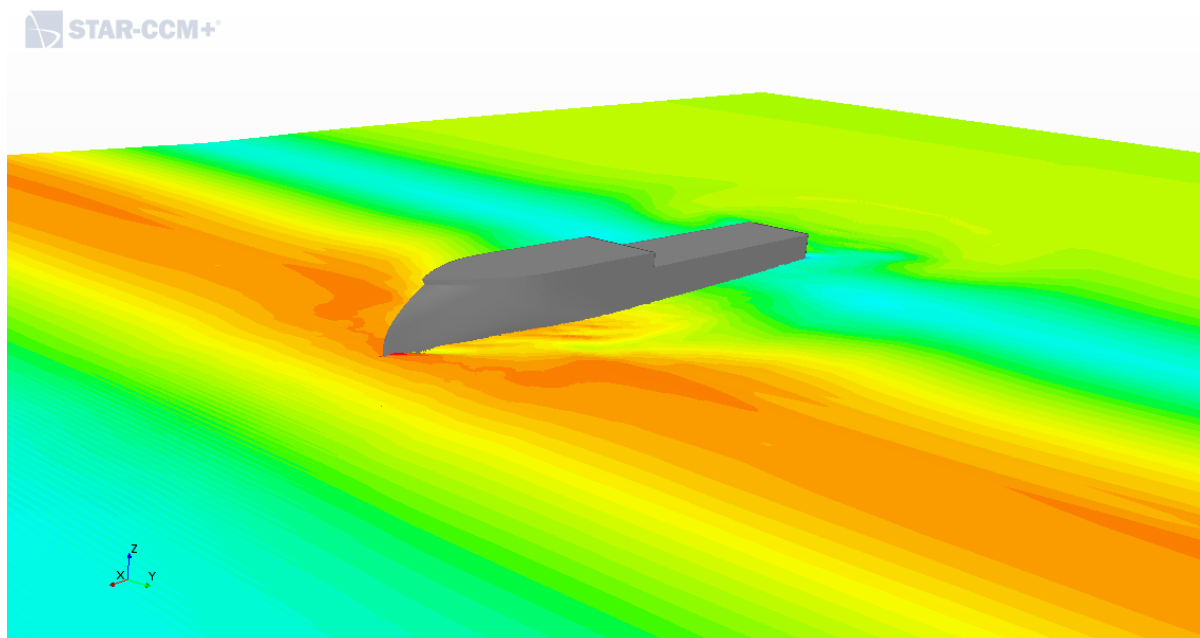


Figure 4.10: Ship Motion Study

## 4.3.1 Heave and Pitch Motions

Figure 4.11 is a combined plot of the heave motion and pitch degree for the modified design, measured in the center of gravity (x=0). The ship was facing waves with 215 meters length and 3 meters height. In the beginning, the solver experienced some disturbances, but throughout the simulation, the pitch motion stabilized. The plot shows that when the heave motion is at its largest, the pitch degree is at its minimum. This is visualized in Figure 4.12 and 4.13. Figure 4.12 shows the ship experiencing a large heave motion, but minimum pitch motion, while the ship in Figure 4.13 is experiencing maximum pitch motion and minimum heave motion.
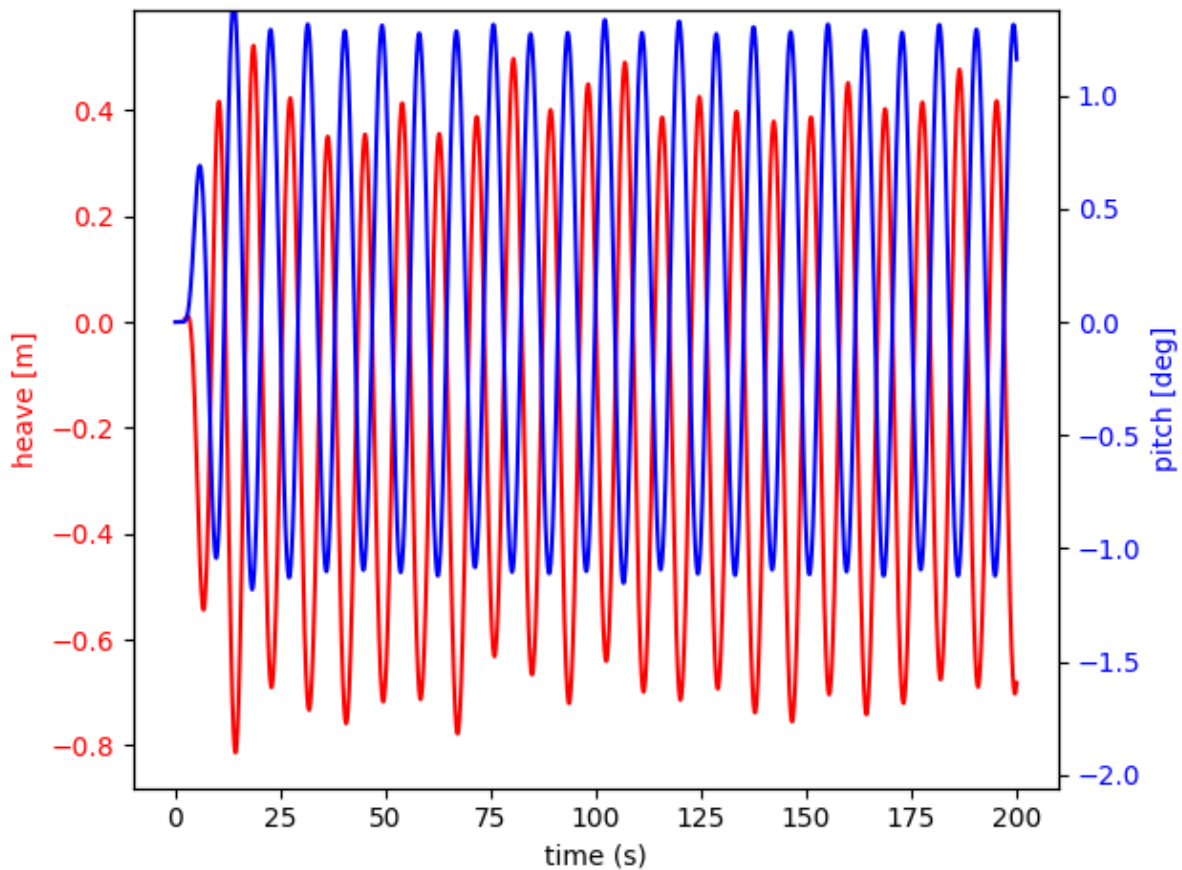


Figure 4.11: Heave Motion and Pitch Degree
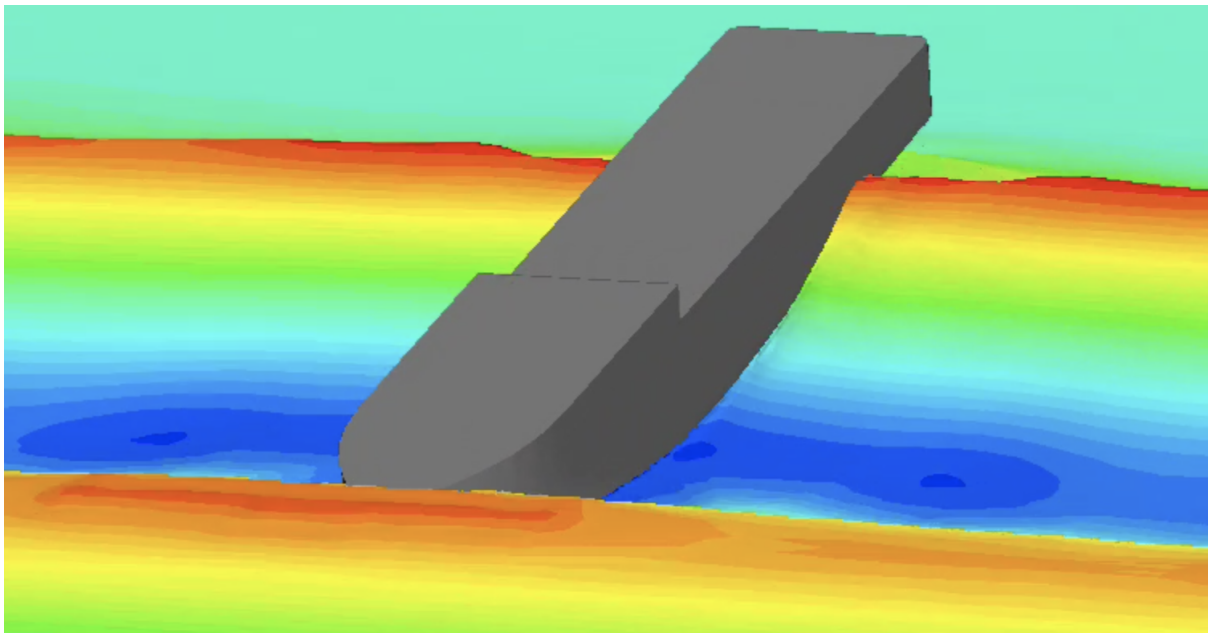
Figure 4.12: Maximum Pitch Motion
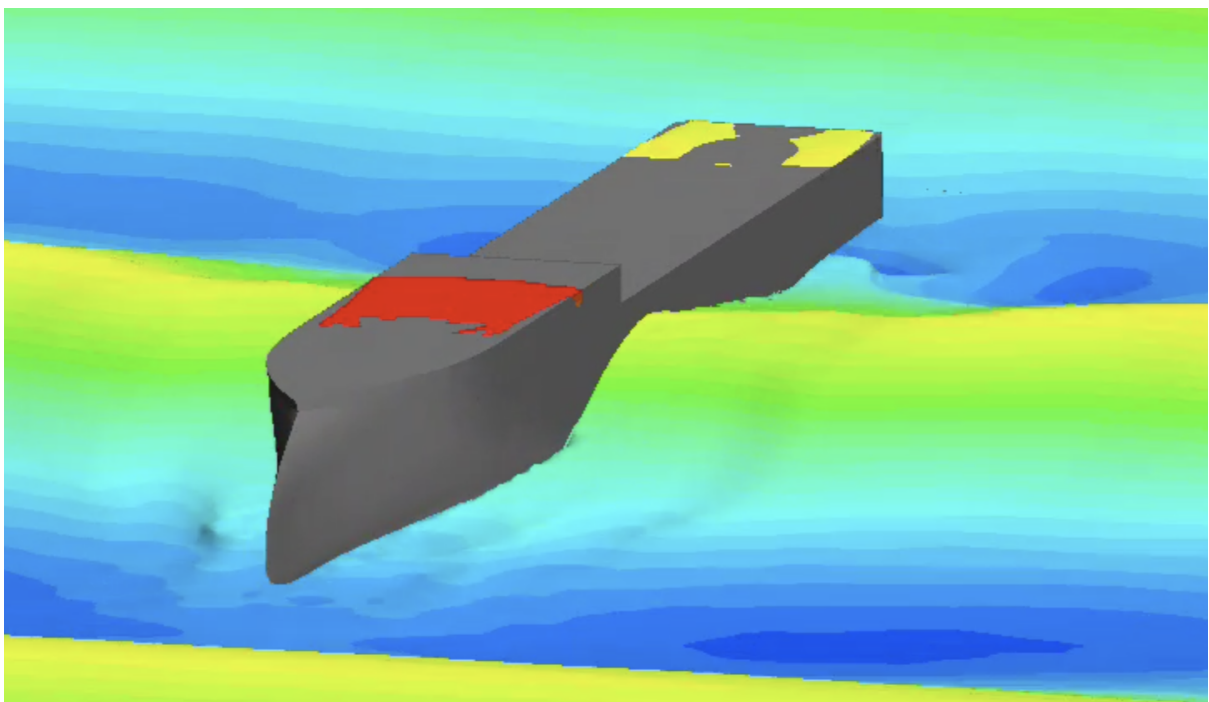


Figure 4.13: Maximum Heave Motion

## 4.3.2 Vertical Accelerations

As mentioned, the heave and pitch motions in the center of gravity was measured. Based in this, the vertical motion, velocity and acceleration was found, and the vertical acceleration was used as a comparison between the two designs. This was done for every wave case in both x=0 and x=100. Figure 4.14 shows the comparison of the two vessels throughout the entire simulation in a wave condition with wave lengths of 320 meters and wave heights of 3 meters, measured 100 meters forward from the center of gravity. The red line shows the accelerations for Design 1, and the blue line shows the acceleration for Design 2. Figure 4.15 is a close up that shows a part of the same plot.
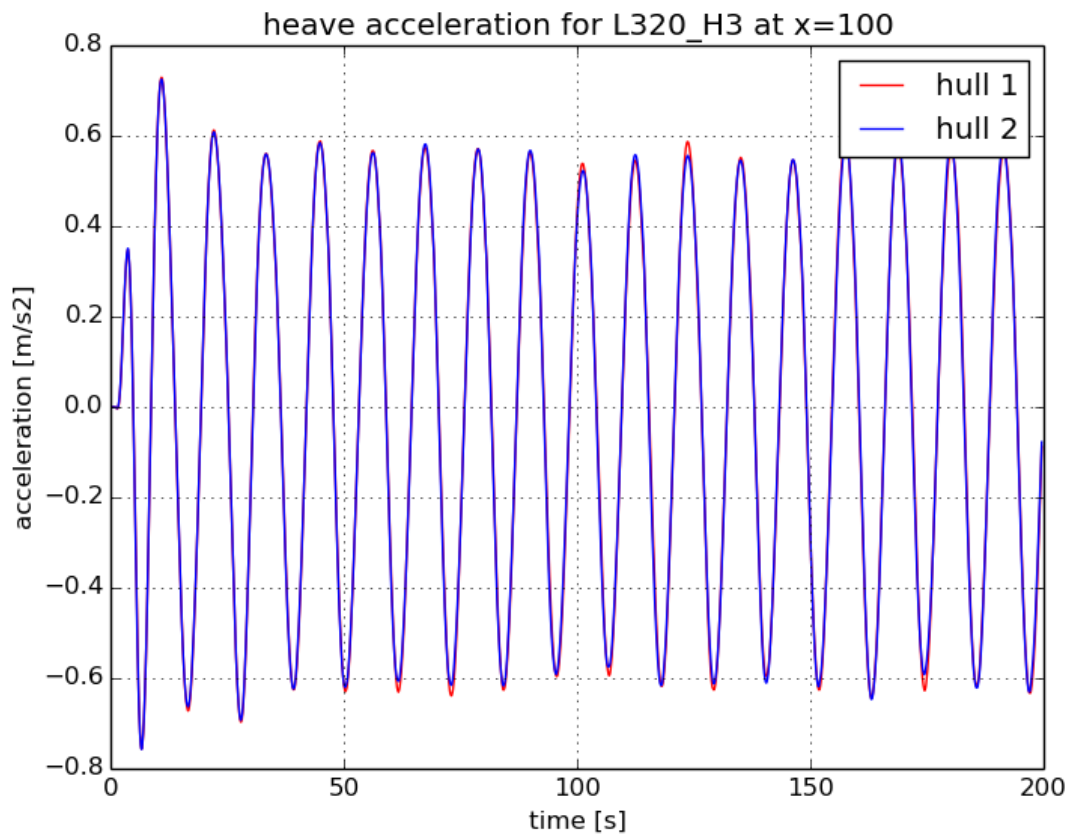


Figure 4.14: Comparison of Vessels with Wave Length 320 m
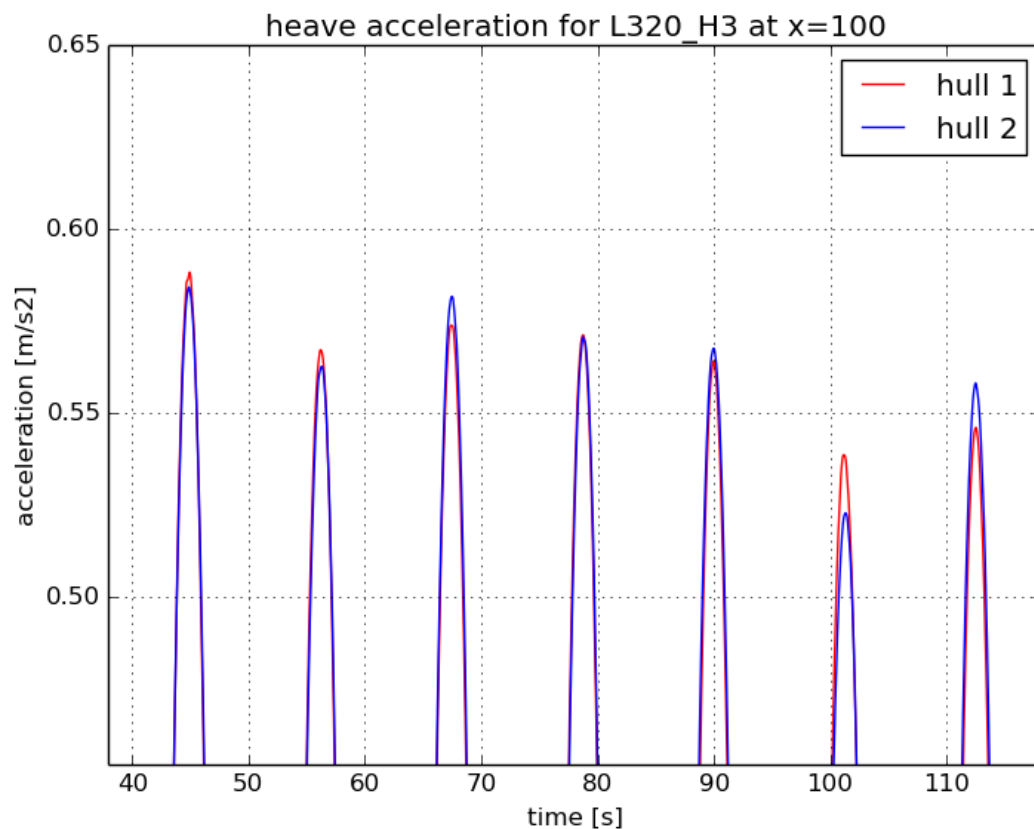
Figure 4.15: Close Up of Comparison of Vessels with Wave Length 320 m

The figures shows that there was no noticeable and constant difference between the vessels in this wave condition. This was also the case for the other wave cases with wave height of 3 meters and 6 meters. The reasons why the effects of the bulbous bow did not show in the results, could be that the mesh was too coarse, so with such a small bulb, the solver was not able to capture the volume change. The plots for the rest of the cases are found in Appendix B.

**Extreme Wave Case**

Figure 4.16 shows the comparison of the two vessels in an extreme case with waves of 200 meters length and 20 meters height. The plot shows a slight difference between the vessels, and from the short time peaks one can see that there are some slamming, caused by the combination of the heave and the forward motion of the ship. The acceleration of the modified hull starts a bit earlier and does not reach a maximum and minimum point as large as the original design, due to increased buoyancy in the fore ship section. This is not a strong argument for the new design as this is only one case, but it may show that the modification is going in the right direction.
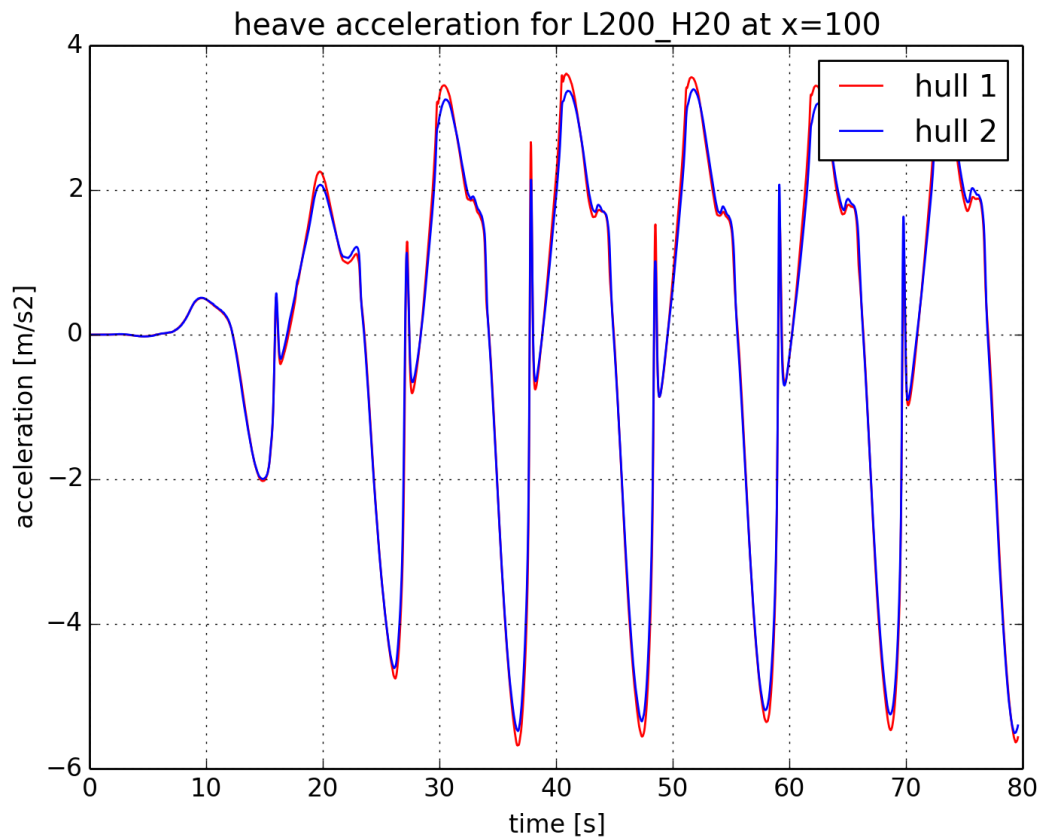


Figure 4.16: Acceleration Comparison with Wave Height = 20m

Figure 4.17 to 4.20 shows the modified hull in the from the simulation with 20 meters high waves. Figure 4.17 and 4.19 shows the ship in a position where the submerged volume is symmetrical. Waves with heights as large as this can cause the submerged volume to be asymmetrical, as Figure 4.18 and 4.20 shows. Here, the submerged volume is either in the bow area or in the stern area.
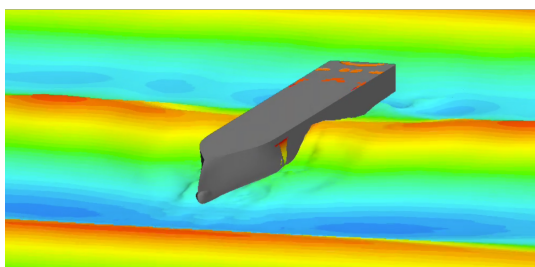


Figure 4.17: Symmetrical
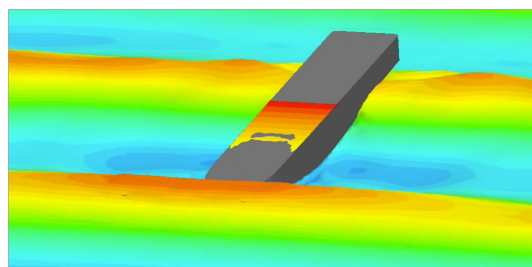


Figure 4.18: Asymmetrically
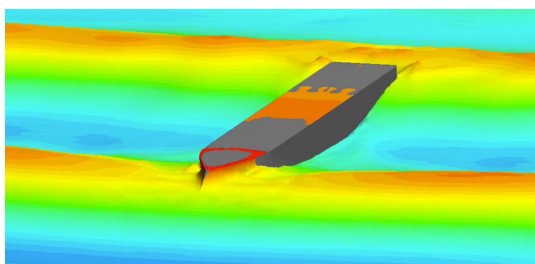


Figure 4.19: Symmetrical
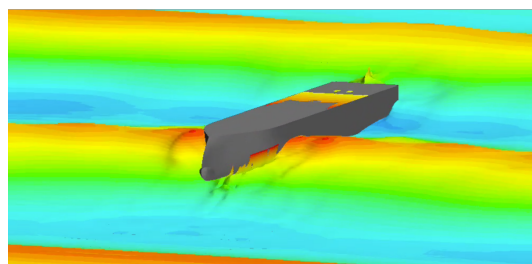


Figure 4.20: Asymmetrically

## 4.4 Uncertainties

When reproducing real states and surroundings computationally, there will be some uncertainties. It is therefore important to have a critical view of the results. With CFD simulations, one may produce results with a various degree of accuracy, but even if they are not precicely correct, the results can be used to capture trends and for comparison of results.

One thing that is highly relevant when running CFD simulations, is the available resources, such as RAM memory, processing capabilities and computational time. Even with a large computational time, it will not be possible to solve a problem that is too computational demanding for the solver. With the resources available for this thesis, one should look at the results with a critical eye. In order to obtain more accurate and reliable results, the total cell amount should probably be at least 10 times as high, something that would require a lot more memory and processing capabilities.

# Chapter 5

# Conclusion

The objective of this thesis was to look at the opportunity to establish a procedure of using results from CFD simulations in every day design in order to modify a ship hull. During the study, a lot of simulations has been run, resulting in a total of seven different cases for each design to be compared. Star CCM+ was chosen to use for the simulations after considering other CFD softwares. A collaboration abroad was also carried out, but due to the circumstances considering COVID-19, the plans needed to be adjusted.

During the simulations, the heave and pitch motions for each vessel was measured. The time series for these two motions was further combined and derived to calculate the vertical acceleration in the center of rotation and 100 meters forward, the location that would experience the greatest accelerations. The simulations was performed with limited resources, and was processed on 8 cores. With more time and better computational resources, the results could have been more accurate, and it would have been possible to propose a new and stronger modification, and repeat the analysis.

The final results shows a slight increase in resistance for the modified vessel. Considering the ship motions, the wanted improvement was not visible for most of the cases due to moderate design changes. In addition to a modest design change, this is justified by a too rough solver that was not able to capture the volume change. But for the case with a wave height of 20 meters, the results shows that the modified design has a lower maximum vertical acceleration, which could indicate that the modification is going in the right direction. With a more drastic design change, the difference may have been visible

for the other wave cases as well, but this would again affect other ship properties which might have severe consequences.

This discussion comes down to answering the research questions. The first research question, *"What are the relevant bow designs with respect to seaworthiness?"*, which led to the modified design in this thesis. A vessels seaworthiness is a broad expression, which was in this thesis narrowed down to the focus around the vessels resistance and vertical acceleration. To create a design to improve these performance factors in such a limited time is not realistic and was neither the objective, but to evaluate the presence of a bulbous bow on an inverted bow design, where both solutions may contribute to improved sea performance.

The second research question raised was *"How can CFD simulations be used to assess seaworthiness?"*, which was the main part of the methodology for this study. The procedure shows that the CFD simulations could be included in an early stage of the design process and used as a tool to improve a design by running simulations, analyze the results, modify the design and repeat the process. For this to be an effective and time saving tool, good computational resources is required.

The last research question was: *"How can performance increase be quantified?"*, and in this study, the performance increase was based on the calm water resistance and the vertical acceleration experienced on board the vessel. This is a small part of the performance of a vessel, and with more time it would have been interesting to look at other parts of this expression, such as the vessels roll motion as well. These performance factors can be used as a comparison between different designs as in this study, but also against international requirements regarding seakeeping, which is important in ship design. As several assumptions was made for the designs, it was not relevant to evaluate the results against international recommendations. It would be interesting to do the same procedure for an operating vessel, and then evaluate against international performance criteria.

As this is an ongoing research effort, it is not easy to draw a final conclusion based on the results. Better resources that could provide a finer solver and more tests are therefore recommended. Ulsteins inverted bow X-Bow® is renowned for its seaworthiness and the improvement in comfort onboard that is linked to this design. The current study seems to show that local modifications of the design can lead to further improvement of these seakeeping abilities, indicating that careful design adjustments may be relevant to adapt the bow to new ship types, and that CFD may be an efficient tool to assess these adjustments. In the present study a bulb was used, but it should be noted that other volume distributions variations of a real X-Bow® may lead to the same, or better, results after careful optimization.

# Chapter 6

# Future Work

The research of this study have found potential to use CFD simulations as a tool for every day design, but this is an ongoing research effort, and there are a lot of things to look further into before a final conclusion could be drawn. The recommendations for further work are listed below:

- More wave cases should be simulated to get a broader image of the ships seaworthiness. The tests in this study was performed in head waves, but to expand the evaluation of seaworthiness by including oblique waves with different attack angles would make the results more trustworthy.

- The term performance factors are in this study narrowed down to resistance and vertical acceleration, which involves heave and pitch motion. Other factors to look further into could be lateral acceleration, roll motion, slamming and deck wetness.

- In this study, the fore ship section was changed. This will also have an impact on the aft section of the vessel, including the inflow to the propeller. The impact the design changes in the fore ship have on the stern section should be investigated, perhaps by using CFD simulations to investigate the ships streamlines.

- To improve the results of the analysis, it would have been beneficial to get simulation time on a cluster that could provide a higher number of cores, so the results would not be limited by time and a too coarse mesh.

# Bibliography

[1] Volker Bertram. *ULSTEIN INTRODUCES THE X-BOW® IN 'COMPACT CONCEPT' ROPAX DESIGNS*. URL: `https://ulstein.com/news/2019/ulstein-introduces-the-x-bow-in-compact-concept-ropax-designs`. (accessed: 2019).

[2] Ulstein Design and Solutions AS. *CFD SIMULATIONS*. URL: `https://ulstein.com/ship-design/customised-designs/cfd-simulations`.

[3] Ulstein Design and Solutions AS. *Innovation - X-Bow*. URL: `https://ulstein.com/innovations/x-bow`. (accessed: 02.03.2017).

[4] Ulstein Design and Solutions AS. *Bourbon Orca*. URL: `https://ulstein.com/references/bourbon-orca`.

[5] Ulstein Design and Solutions AS. *TANK TEST AND REAL-LIFE COMPARISON*. URL: `https://ulstein.com/innovations/x-bow/comparison-tests`.

[6] Soumya Chakraborty. *What's The Importance Of Bulbous Bow Of Ships?* URL: `https://www.marineinsight.com/naval-architecture/why-do-ships-have-bulbous-bow/`. (accessed: 04.10.2019).

[7] Manuel Venture. *Ship Design - Bulbous Bow Designs and Construction*.

[8] Tetsuo Yanagida - Monohakobi Technology Institute. *Challenge for Hull-Form Optimization Tailored to Actual Operation Environments*. URL: `https://www.monohakobi.com/en/news/mtijournal/yanagida/`.

[9] F.Lopez Pena C.Guedes Soares. *Developments in Maritime Transportation and Exploitation of Sea Resources*. Vol. 1. CRC Press, 2014. ISBN: 978-1-138-00124-4.

[10]  Volker Bertram. *Practical Ship Hydrodynamics (Second Edition) - Ship Seakeeping*. URL: `http://www-cs-faculty.stanford.edu/~uno/abcde.html`. (accessed: 2012).

[11]  Yutaka Tanaka. *Active vibration compensator on moving vessel by hydraulic parallel mechanism*. URL: `https://www.researchgate.net/publication/327901742_Active_vibration_compensator_on_moving_vessel_by_hydraulic_parallel_mechanism`. (accessed: 01.2018).

[12]  Ivan R. Nielsen. *Assessment of Ship Performance in a Seaway*. 3rd ed. Sortedam Dossering 19, DK-200 Copenhage, Denmark: NORDFORSK, 1987.

[13]  Versteeg and Malalasekera. *An Introduction to Computational Fluid Dynamics*. 2nd ed. Pearson Education Limited, 2007. ISBN: 978-0-13-127498-3.

[14]  Ferziger and Peric. *Computational Methods for Fluid Dynamics*. 3rd ed. Springer, 2002. ISBN: 3-540-42074-6.

[15]  Wangda Zuo. *Introduction of Computational Fluid Dynamics*. URL: `http://wwwmayr.informatik.tu-muenchen.de/konferenzen/Jass05/courses/2/Zuo/Zuo_paper.pdf`.

[16]  Bengt Andersson. *Computational Fluid Dynamics for Engineers*. Cambridge University Press, 2011.

[17]  San Yu Khaing Thet Mon Soe. *Comparison of Turbulence Models for Computational Fluid Dynamics Simulation of Wind Flow on Cluster of Buildings in Mandalay*. 2017. ISBN: 2250-3153.

[18]  F. MoukalledL. ManganiM. Darwish. *The Finite Volume Method in Computational Fluid Dynamics*. Vol. 113. Springer, 2015.

[19]  Udvavisk Technologies. *FINITE VOLUME METHOD FOR COMPUTATIONAL FLUID DYNAMICS (CFD)*. URL: `https://www.udvavisk.com/finite-volume-method/`.

[20]  Simcenter STAR-CCM+. *Star CCM+ Documentation*. URL: `https://documentation.thesteveportal.plm.automation.siemens.com/starccmplus_latest_en/index.html`. (accessed:2019).

[21]   Katsutaka Okamori. *Master Course for Fluid Simulation Analysis of Multi-phase Flows by Oka-san: 3. VOF (volume of fluid) method*. URL: `https://www.cradle-cfd.com/media/column/a105`.

[22]   Clement Kleinstreuer. *Modern Fluid Dynamics*. 2nd ed. Taylor and Francis Group, 2018. ISBN: 978-1-138-19810-4.

[23]   Zeka Mazhar. *Fully Implicit, Coupled Procedures in Computational Fluid Dynamics*. Springer, 2016.

[24]   H. Schlichting and K. Gersten. *Boundary-Layer Theory*. 8th ed. Springer, 2000.

[25]   Timothy J. Baker. *Mesh Movement and Metamorphosis*. 10th International Meshing Roundtable, 2001. ISBN: 3257227892.

# Appendix A

# Refinement Zones



Figure A.1: Hull Refinement - Fine
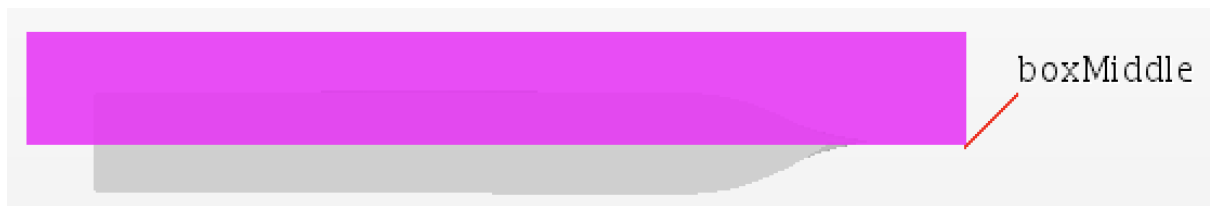


Figure A.2: Hull Refinement - Middle
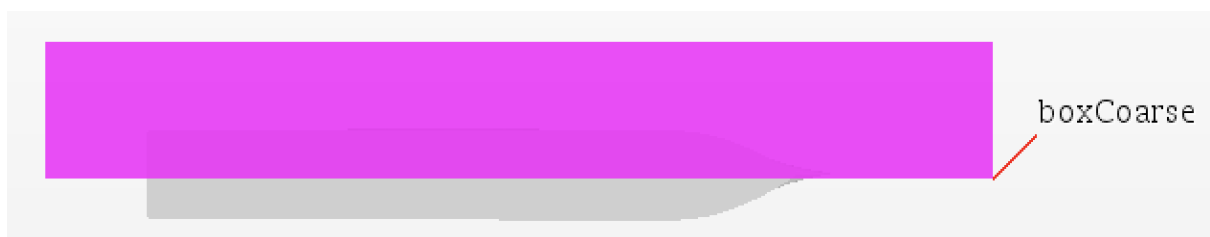


Figure A.3: Hull Refinement - Coarse

Figure A.4: Free Surface Refinement - Fine



Figure A.5: Free Surface Refinement From Above - Fine

# Appendix B

# Simulation Results

## B.1 Calm Water Resistance
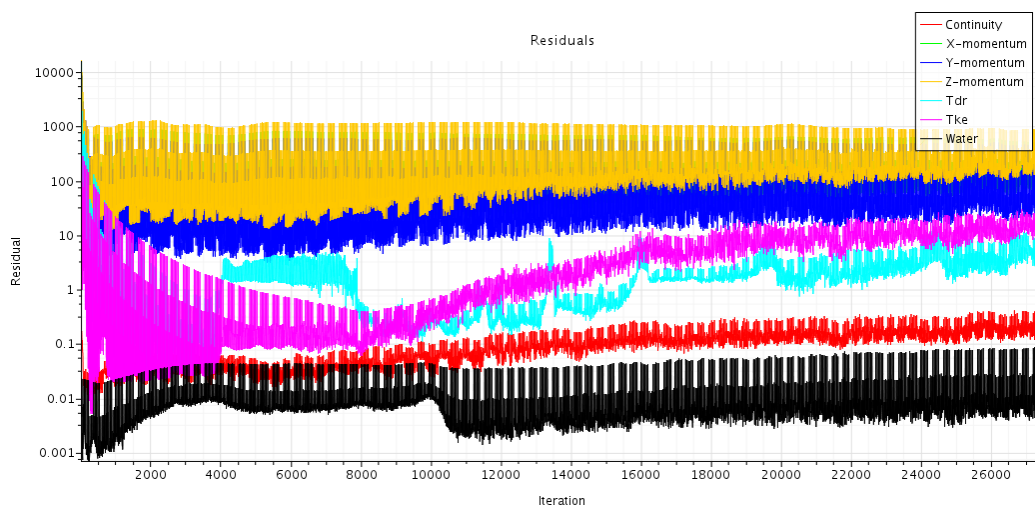


Figure B.1: Resistance: Residuals - Hull 1
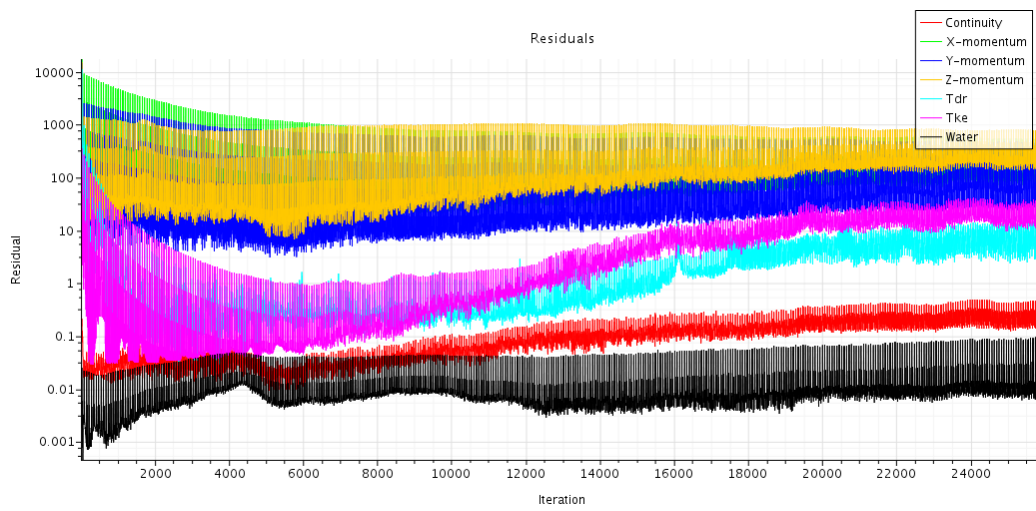
Figure B.2: Resistance: Residuals - Hull 2
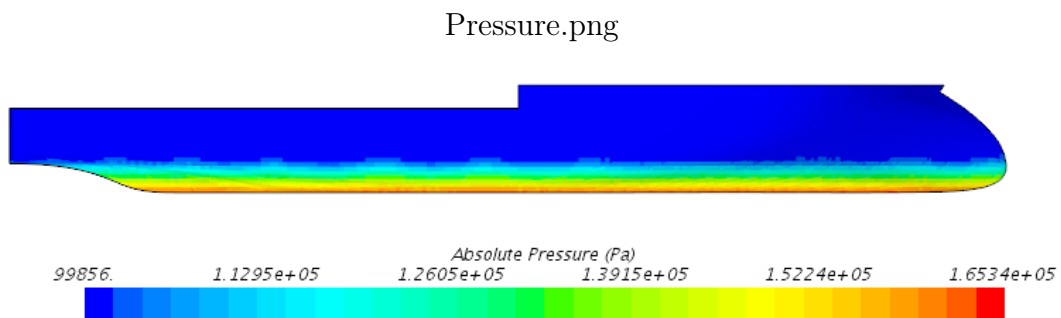
Pressure.png



Figure B.3: Resistance: Absolute Pressure - Hull 1
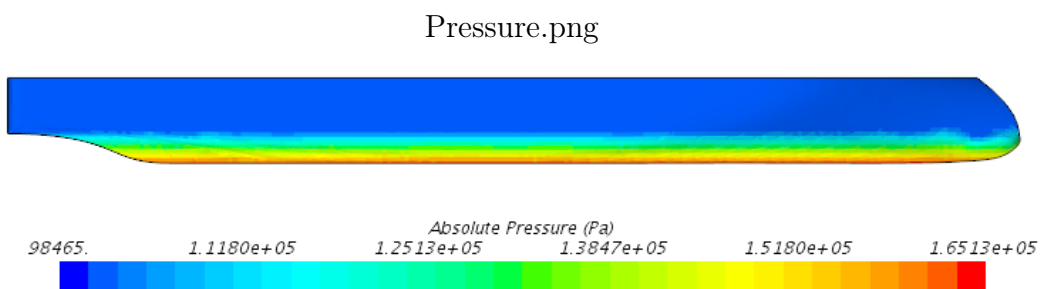
Pressure.png



Figure B.4: Resistance: Absolute Pressure - Hull 2
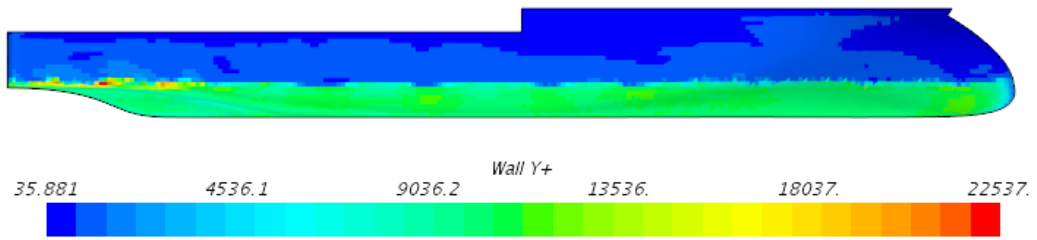
Figure B.5: Resistance: Wall Y+ - Hull 1
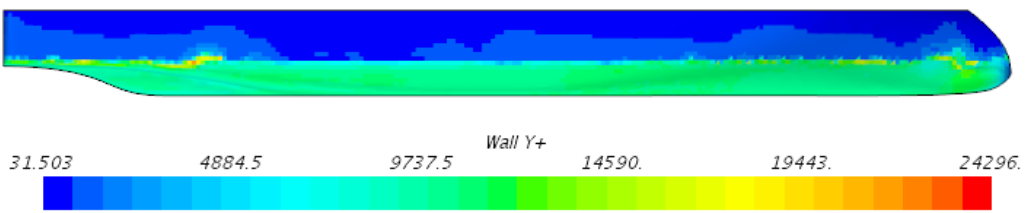


Figure B.6: Resistance: Wall Y+ - Hull 2

## B.2 Ship Motion Study

### B.2.1 Wave Length = 215 meters, Wave Height = 3 meters
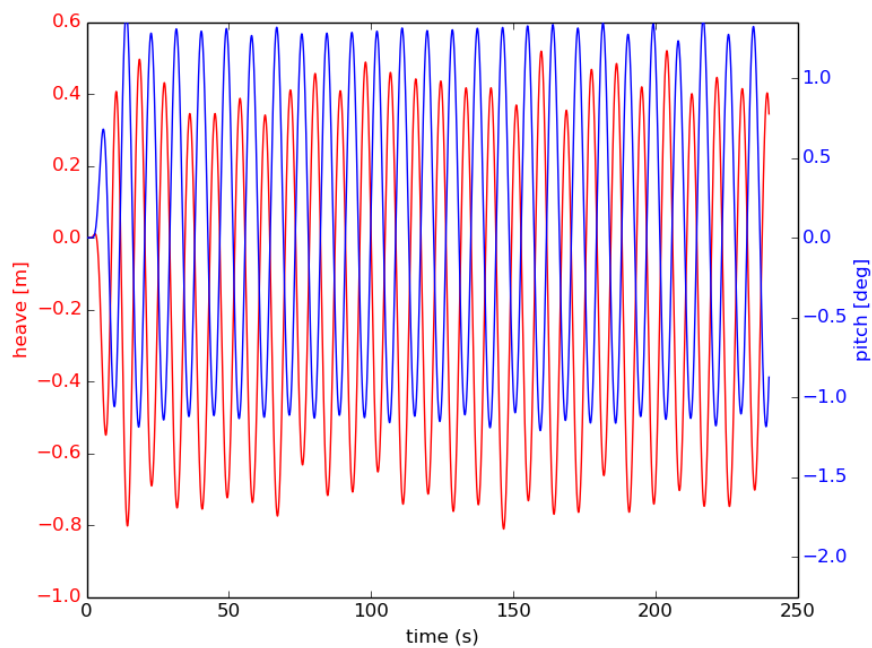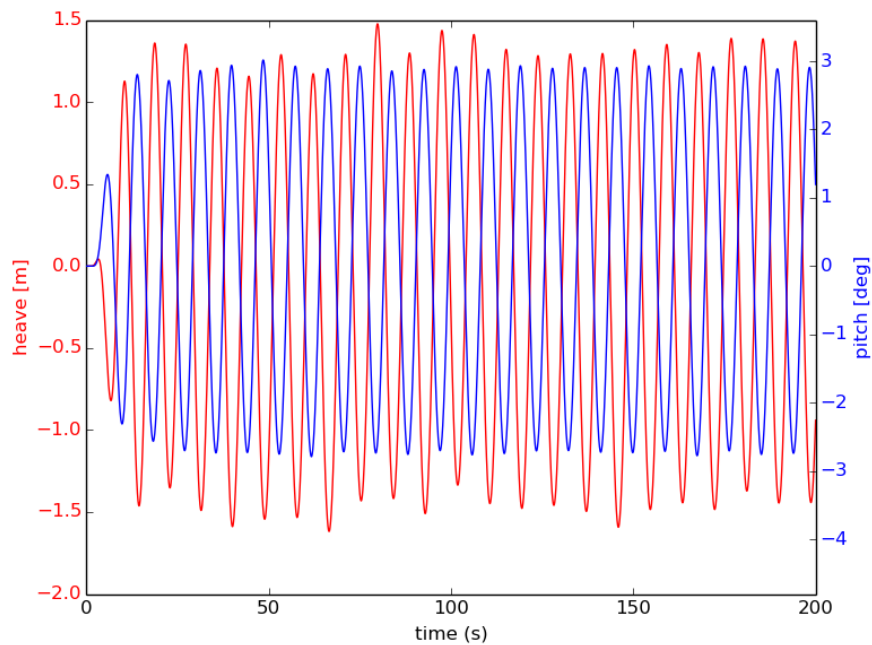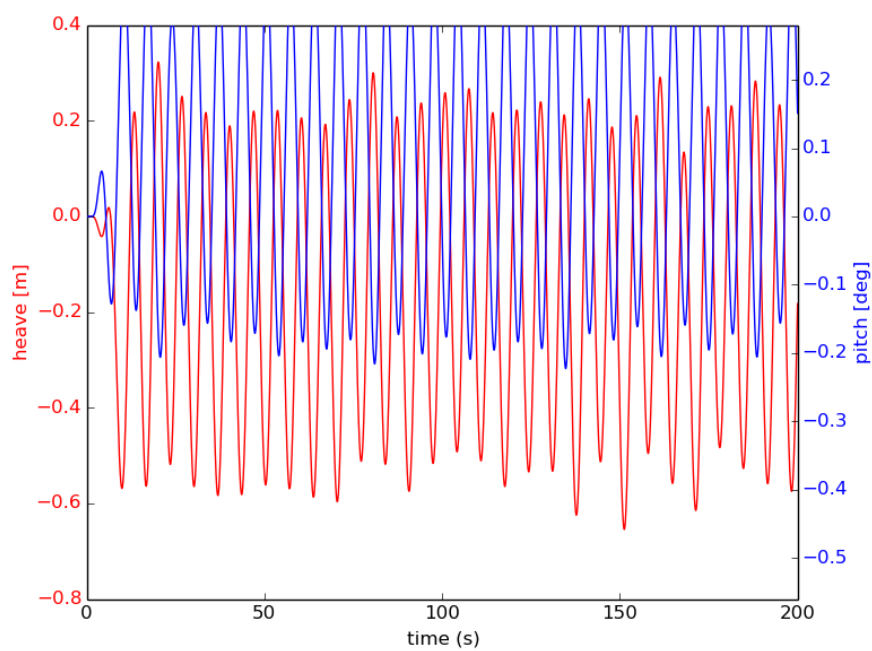


Figure B.7: Heave/Pitch Hull 1
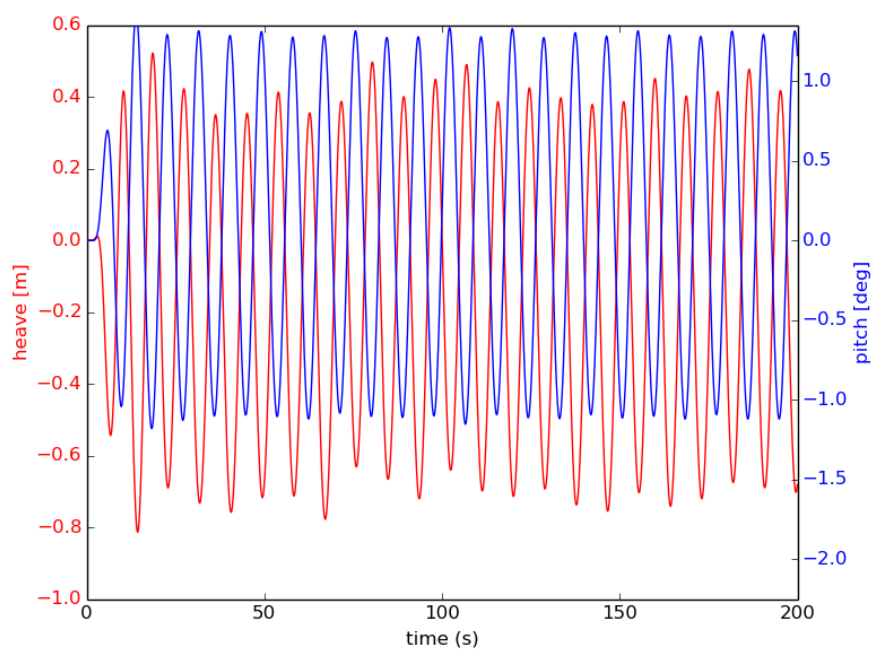


Figure B.8: Heave/Pitch Hull 2
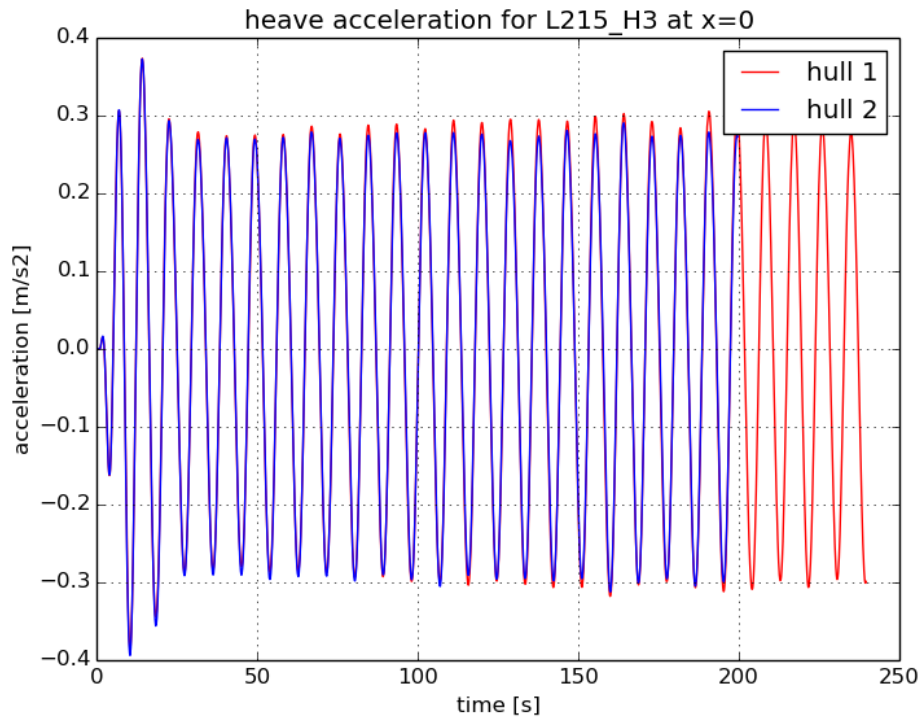
Figure B.9: Vertical Acceleration in CoG
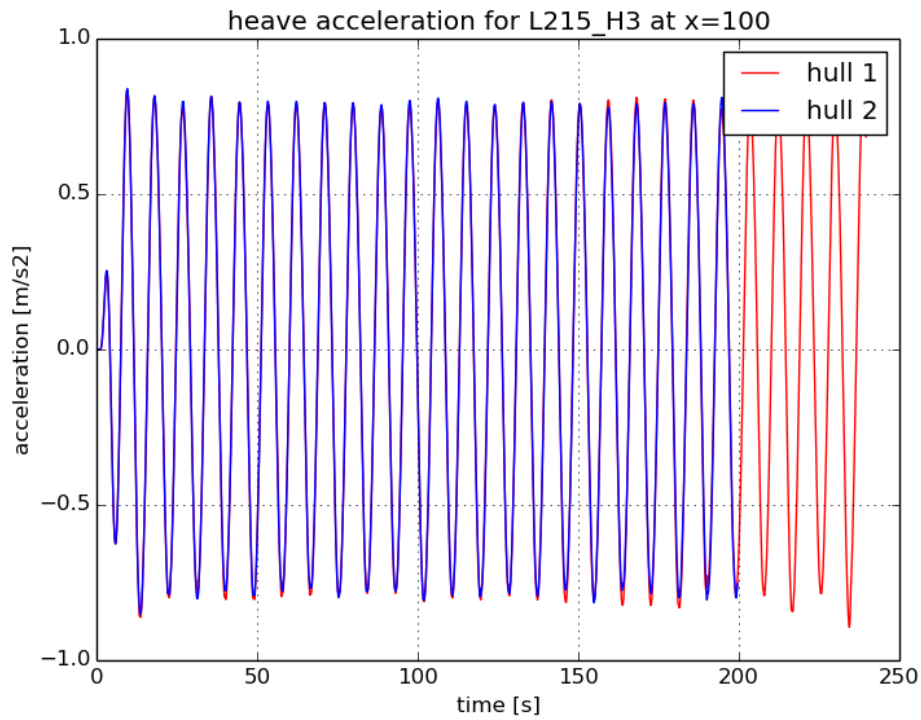


Figure B.10: Vertical Acceleration in x=100

### B.2.2 Wave Length = 320 meters, Wave Height = 3 meters
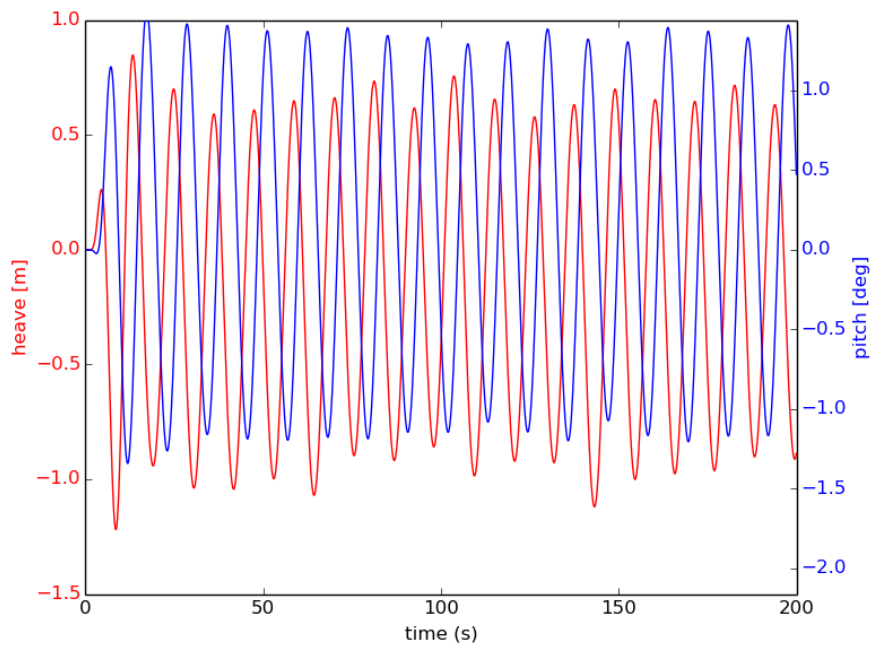


Figure B.11: Heave/Pitch Hull 1
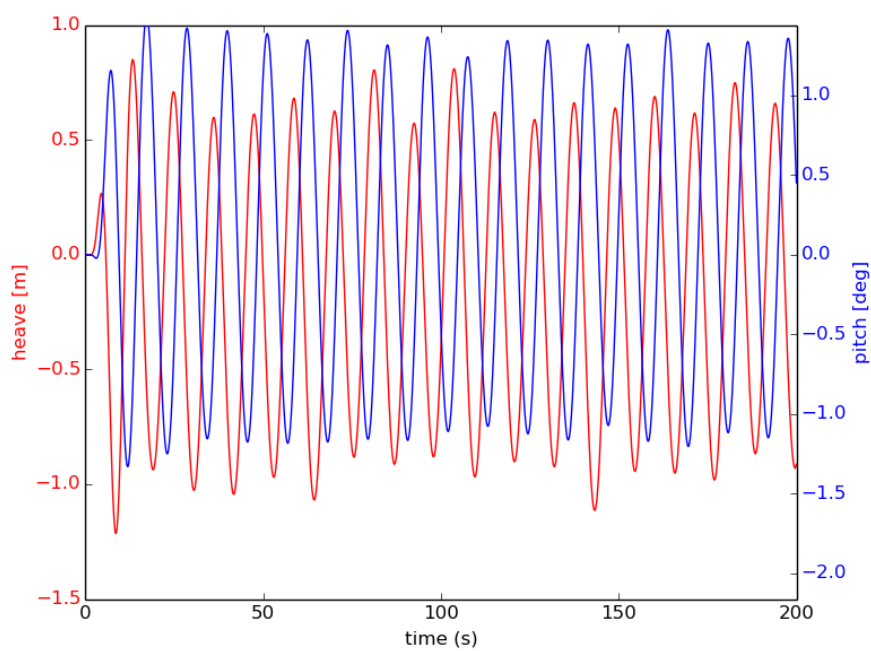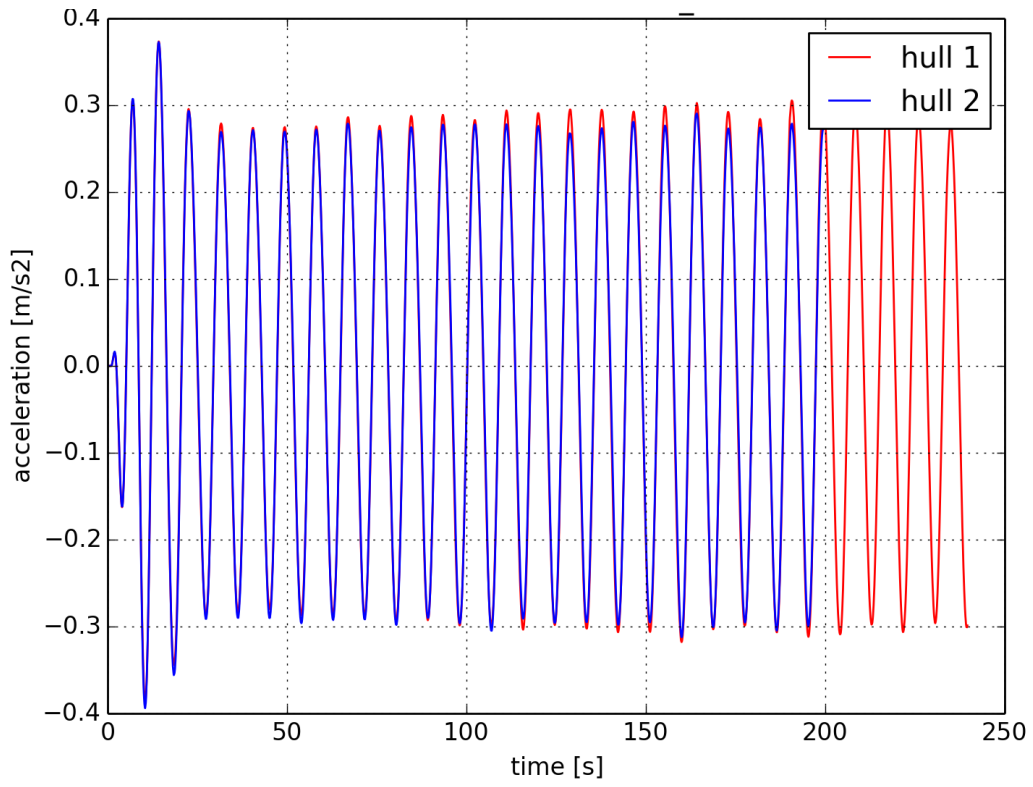


Figure B.12: Heave/Pitch Hull 2
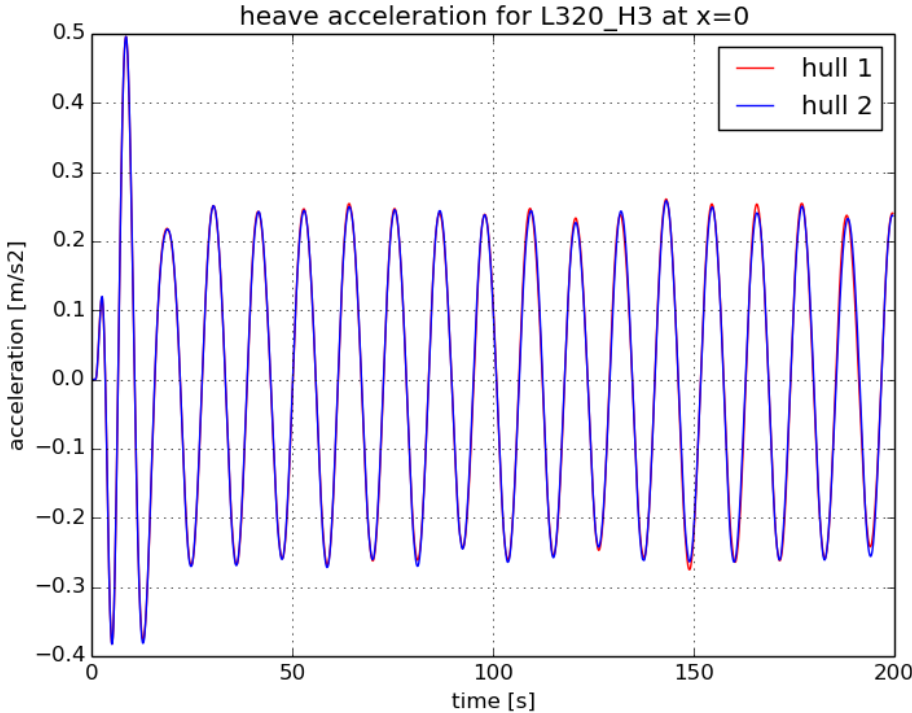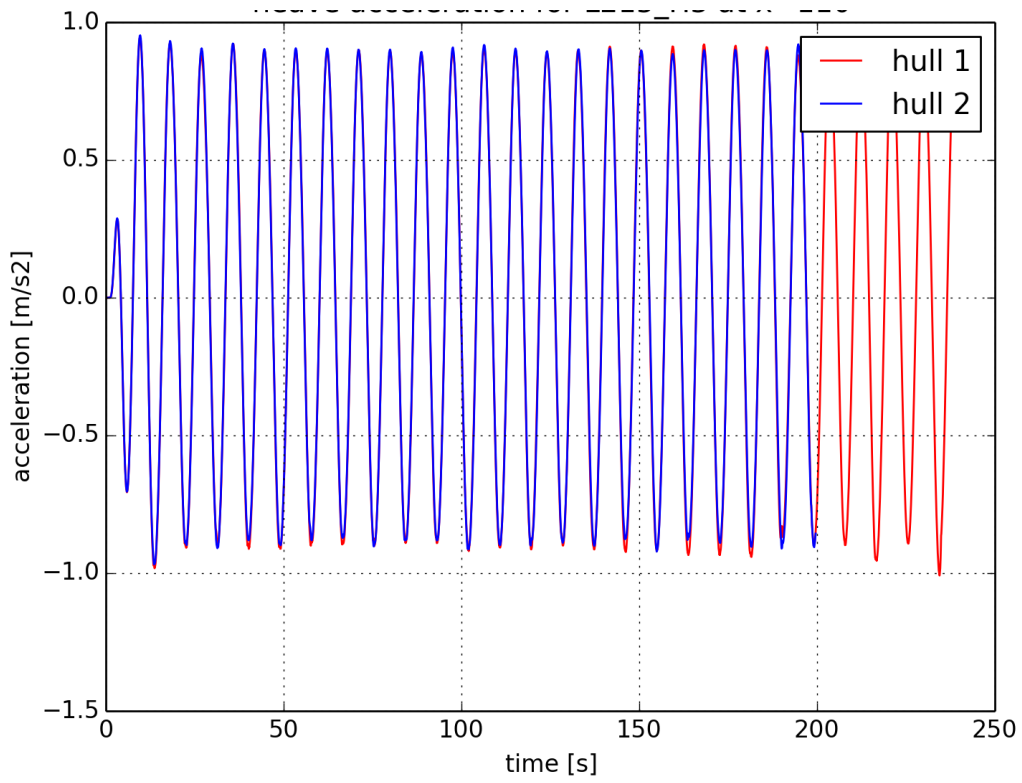
Figure B.13: Vertical Acceleration in CoG
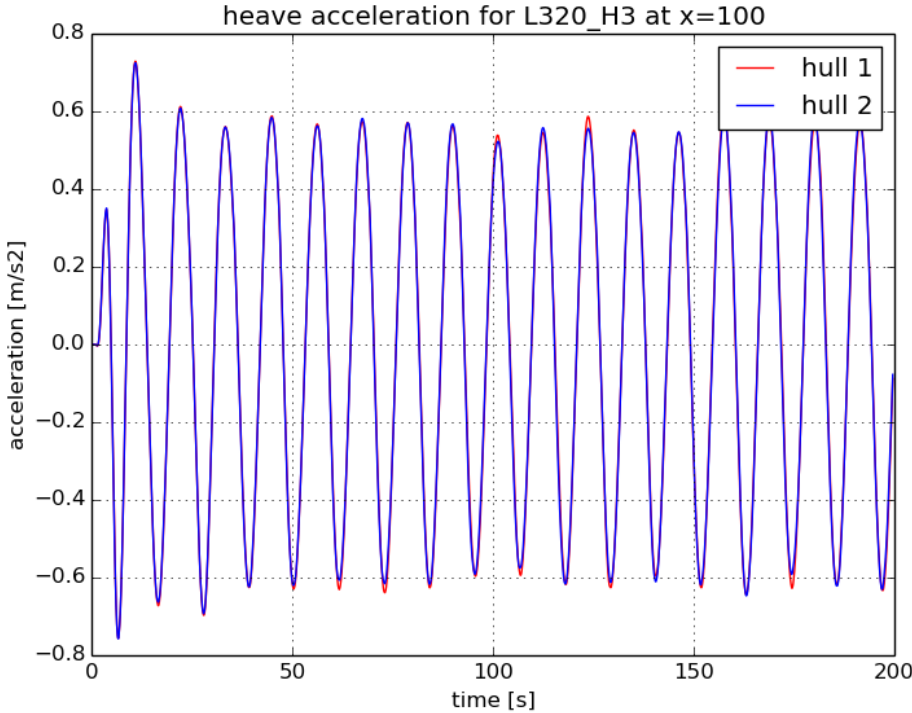


Figure B.14: Vertical Acceleration in x=100

### B.2.3 Wave Length = 140 meters, Wave Height = 3 meters
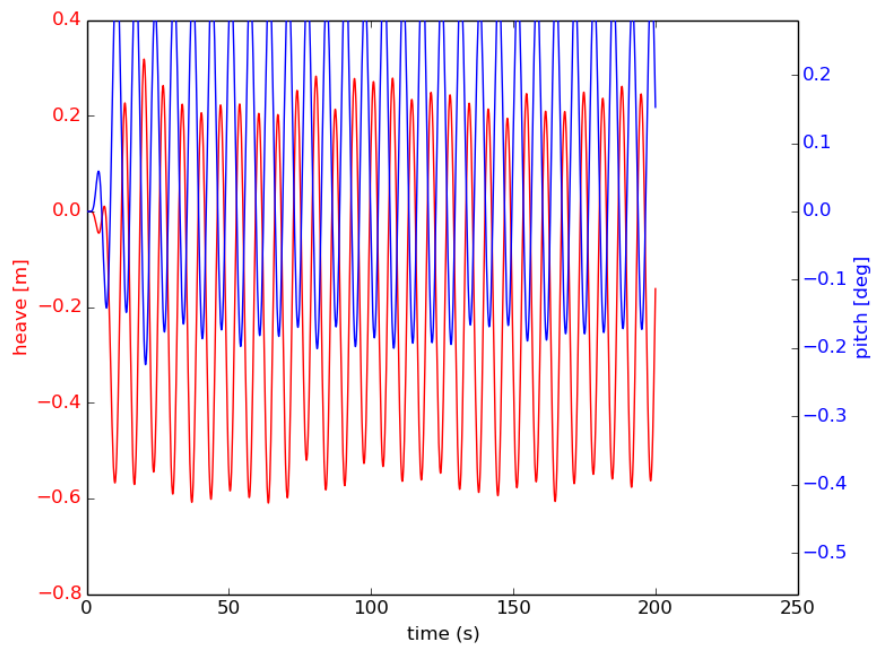


Figure B.15: Heave/Pitch Hull 1
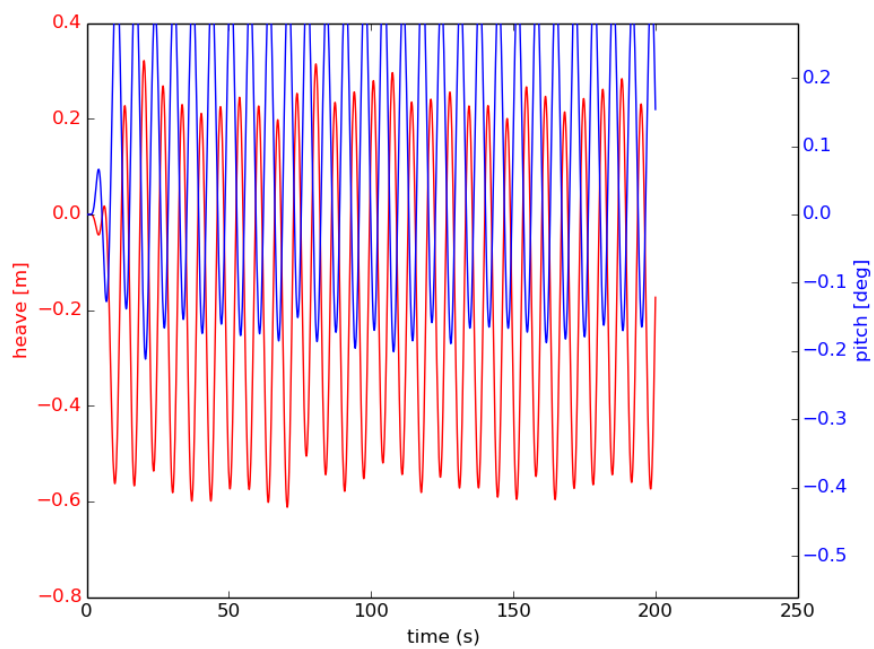


Figure B.16: Heave/Pitch Hull 2
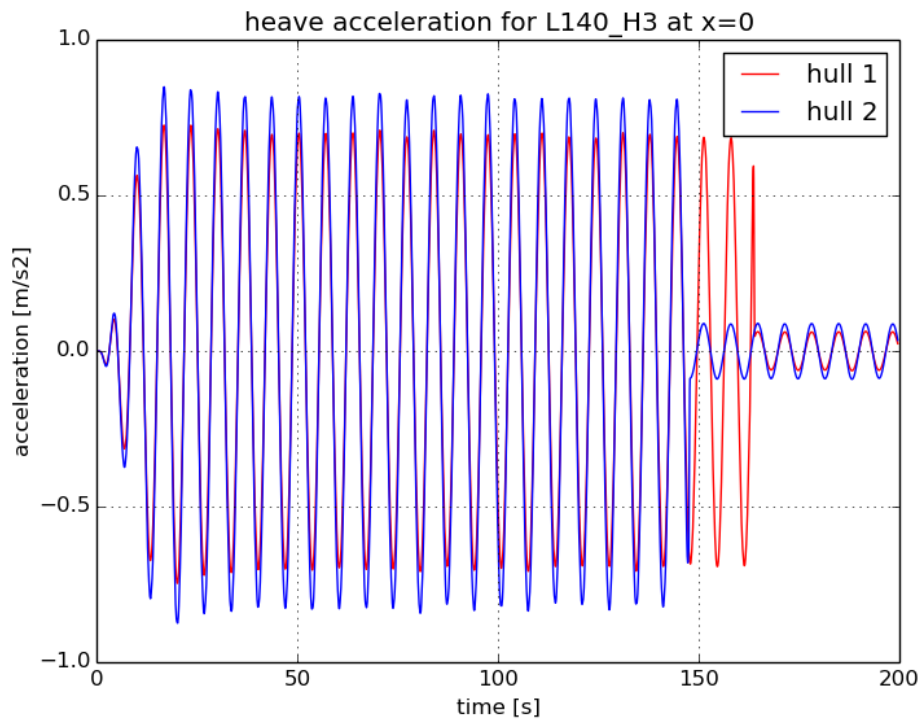
Figure B.17: Vertical Acceleration in CoG
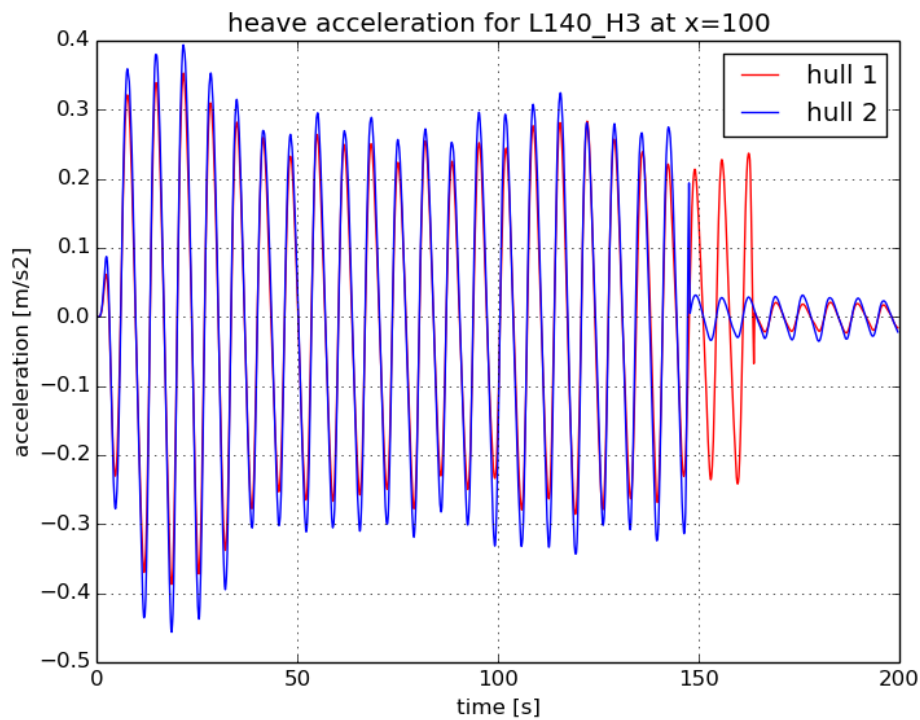


Figure B.18: Vertical Acceleration in x=100

### B.2.4 Wave Length = 105 meters, Wave Height = 3 meters
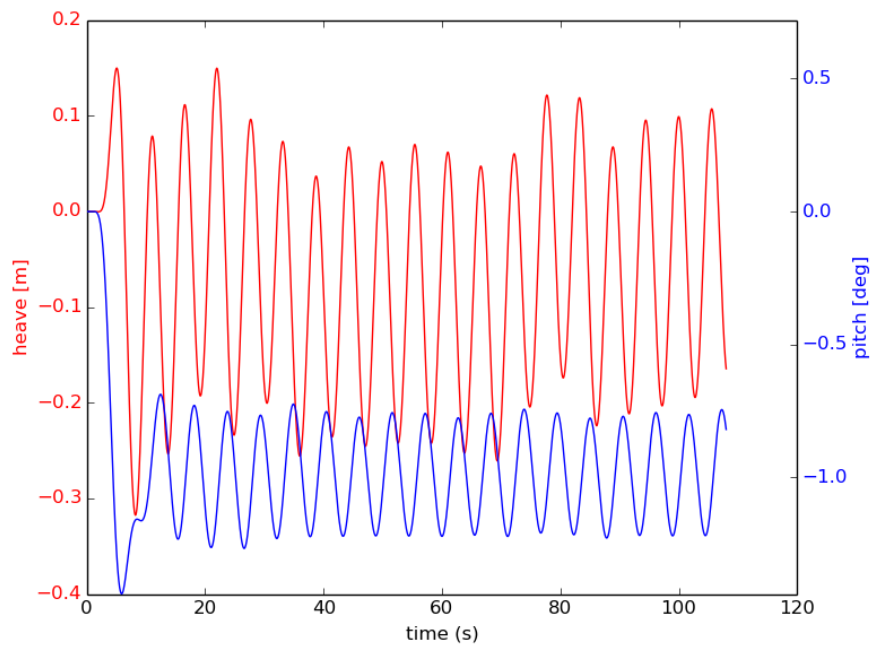


Figure B.19: Heave/Pitch Hull 1
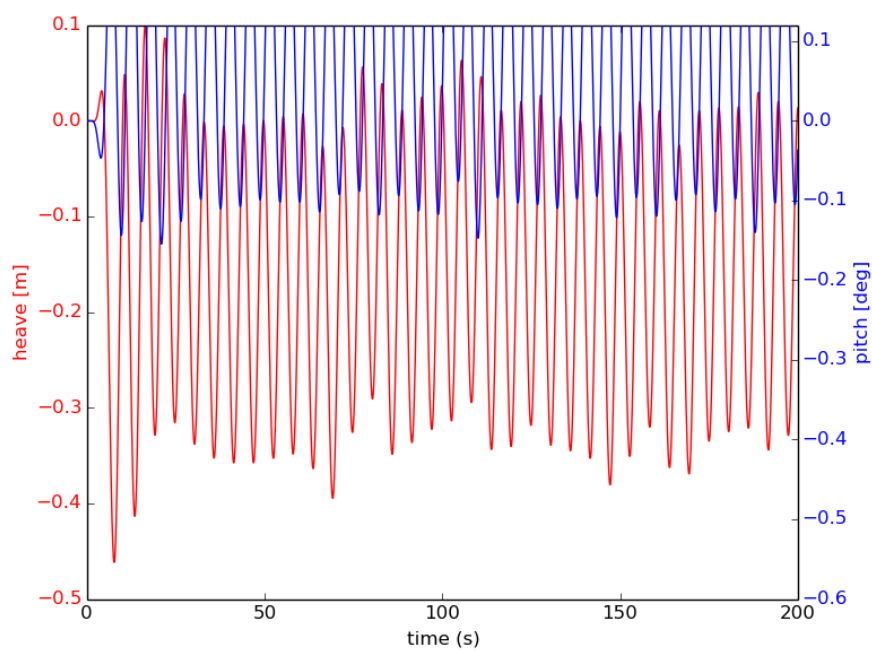


Figure B.20: Heave/Pitch Hull 2
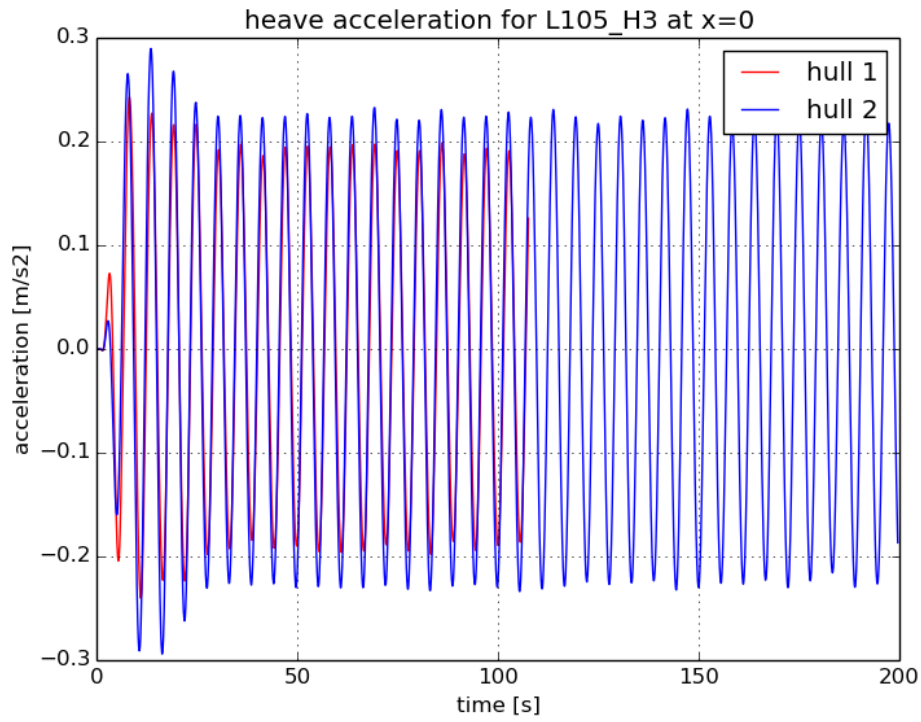
Figure B.21: Vertical Acceleration in CoG
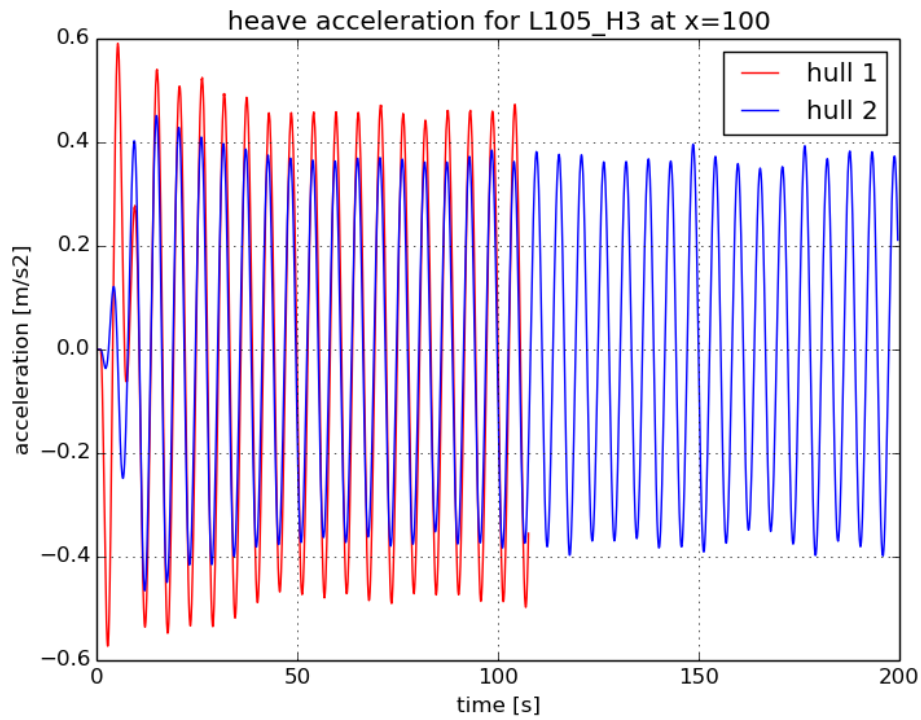


Figure B.22: Vertical Acceleration in x=100

## B.2.5   Wave Length = 215 meters, Wave Height = 6 meters



Figure B.23: Heave/Pitch Hull 1



Figure B.24: Heave/Pitch Hull 2

Figure B.25: Vertical Acceleration in CoG



Figure B.26: Vertical Acceleration in x=100

## B.2.6  Wave Length = 200 meters, Wave Height = 20 meters
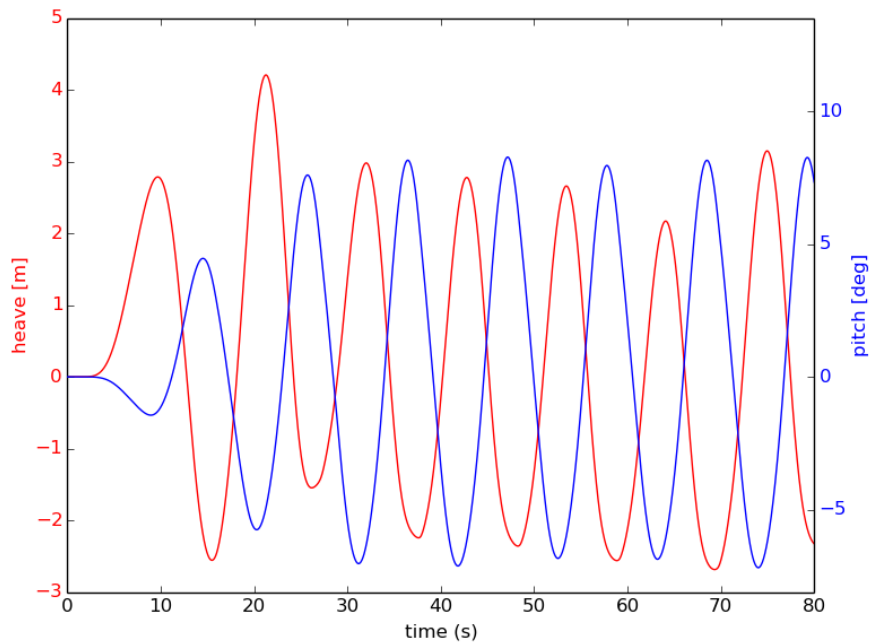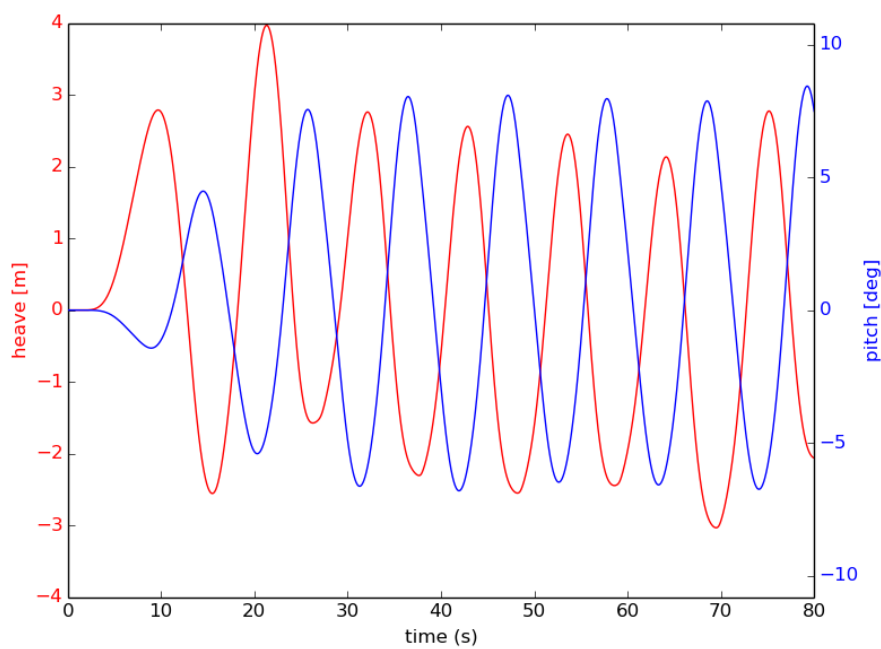


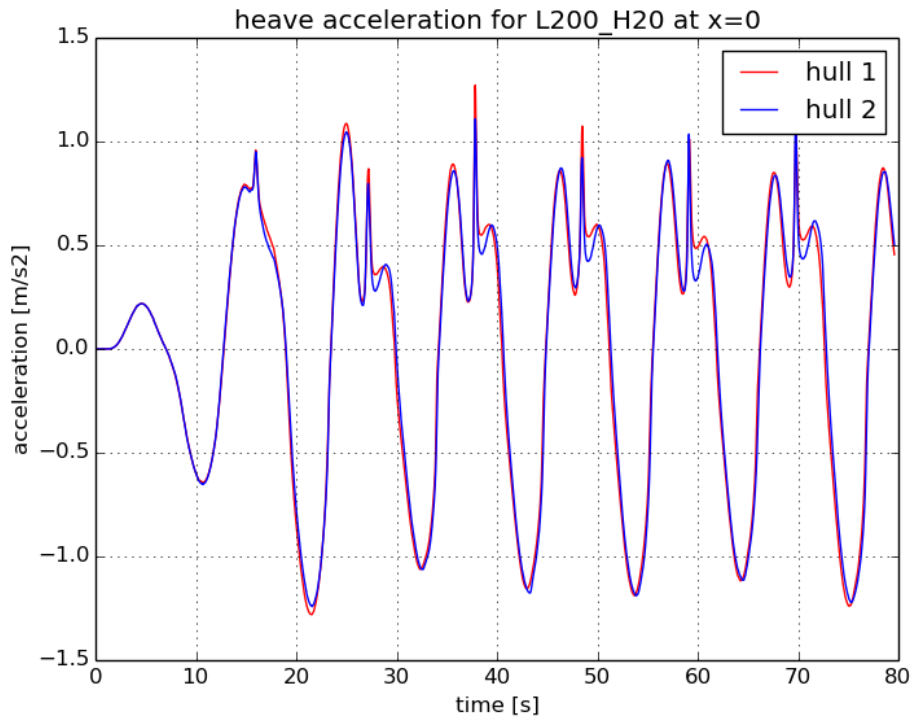Figure B.27: Heave/Pitch Hull 1
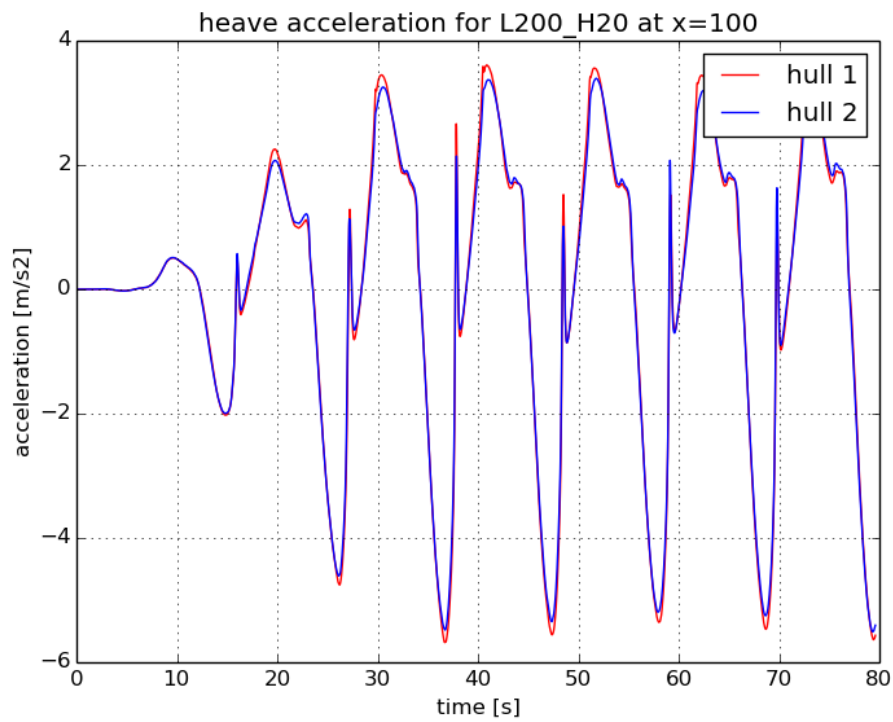


Figure B.28: Heave/Pitch Hull 2

Figure B.29: Vertical Acceleration in CoG



Figure B.30: Vertical Acceleration in x=100